ÉCOLE DE PHYSIQUE DES HOUCHES – UJF & INPG – GRENOBLE

a NATO Advanced Study Institute

LES HOUCHES

SESSION LXXIII

2-28 July 2000

Atomic clusters and nanoparticles

Agrégats atomiques et nanoparticules

Edited by

C. GUET, P. HOBZA, F. SPIEGELMAN and F. DAVID

EDP SCIENCES

Les Ulis, Paris, Cambridge

Springer

Berlin, Heidelberg, New York,
Barcelona, Hong Kong, London
Milan, Paris, Tokyo

Published in cooperation with the NATO Scientific Affair Division

ISBN 3-540-42908-5 Springer-Verlag Berlin Heidelberg New York
ISBN 2-86883-536-8 EDP Sciences Les Ulis

Printed in France

EXCITATIONS IN CLUSTERS

G.F. Bertsch

1 Introduction

There are two points of view on cluster physics, which are implicit when one asks the questions:

> Do the properties of clusters bridge the physics of atoms to the physics of bulk systems?
>
> Or do clusters form a world of their own, with unique properties seen neither in atoms nor in macroscopic systems?

A positive answer to the first question would give a strong motivation to study clusters in order to develop tools for studying large systems. Because clusters are finite with discrete electronic excitations, their observed properties might presumably be used more effectively to develop better theory. On the other hand, a positive answer to the second question is motivation to study clusters in their own right. In fact, depending on the properties under study, both questions have affirmative answers.

One of the unique aspects of clusters is their magic numbers, which will be discussed in detail in the lectures of Martin and Brack. A sampler of abundance spectra showing the magic number phenomena is displayed in Figure 1.

In the top panel are shown the abundances of sodium clusters in the pioneering 1984 experiment of Knight *et al.* [1]. The numbers 8, 20, 40, are clearly favored. These numbers can be associated with the group SU(3). This is a fancy way of saying that the experiment showed special stability for the closed shells in a three-dimensional harmonic oscillator potential, which happens to carry the symmetry of the group SU(3). The most important point is that spherical shell closures of delocalized electrons convey stability to the system and determines structure. In nuclear physics the discovery of shells of delocalized particles opened the door to more powerful theoretical tools to understand nuclear structure, and the same has happened in metal cluster physics.

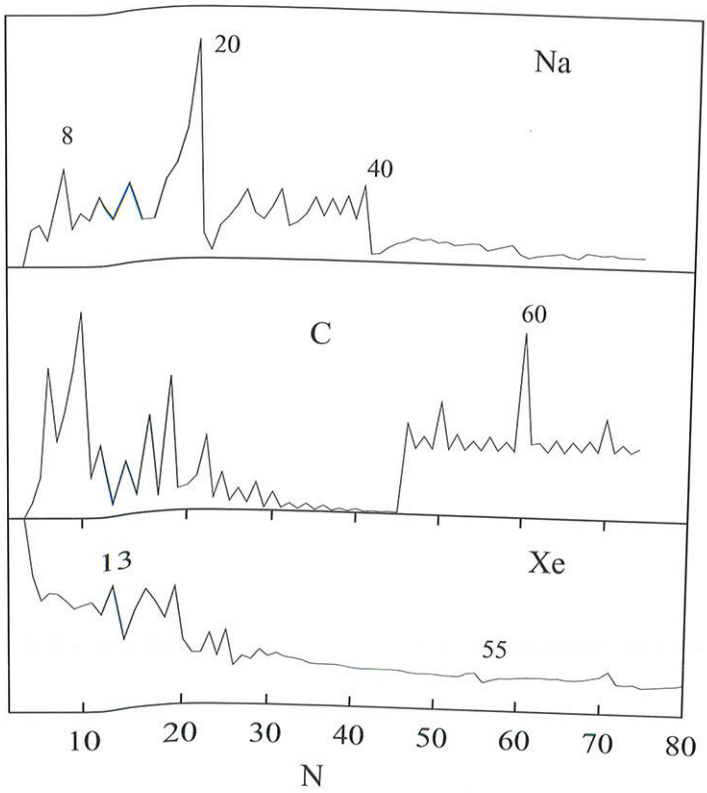

Fig. 1. Abundance spectra in cluster beams. The data are from the following references: carbon [4]; sodium [1]; xenon [3].

Magic numbers of very different origin come from the geometric arrangements of atoms in a cluster. The Mackey icosahedra [2] are the prime example of geometric packing in finite systems. Let us try to pack hard balls into a compact shape. Starting with one at the center, one finds up to twelve can be positioned around the central ball and touching it. However, the packing is imperfect in that the outer layer of balls is not close packed, and contains spaces between at least some of the balls. The space can be arranged symmetrically putting the outer balls at the vertices of an icosahedron. Each face of the icosahedron is defined by a triangle of balls. The Mackey construction adds layers by building a larger triangle on each face. These icosahedral numbers were seen first in a cluster beam experiment on Xe clusters [3], shown in the lower panel of Figure 1. The favored icosahedral numbers are 13, 55, 147, ... However, one sees in this experiment that

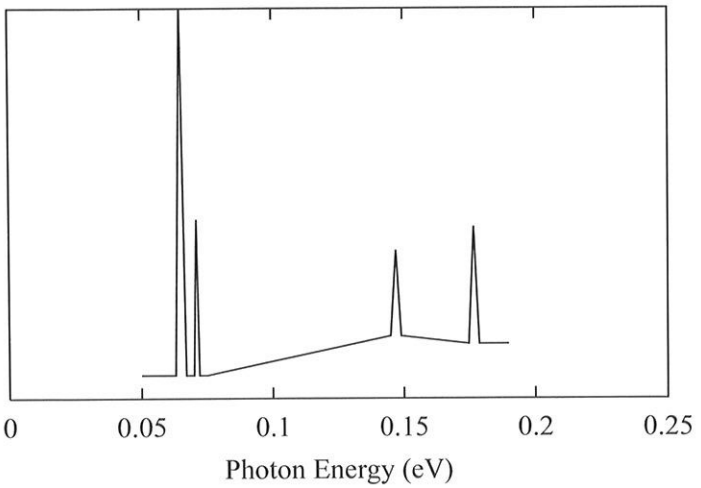

Fig. 2. Schematic infrared absorption spectrum of C_{60}, from reference [5].

the icosahedral numbers hardly stand out from others equally prominent. Martin's lectures will explain how in the basic icosahedral framework other numbers can arise as well.

The middle panel in Figure 1 shows carbon abundances with the famous peak at $N = 60$ from the fullerene molecule C_{60}. In this case, the experimentalists observed that 60 was magic, and deduced from that the structure should be icosahedral, with the carbon atoms positioned like the vertices on a soccer ball. In some respect, C_{60} is an ideal molecule to bridge the atom and the bulk: it is the largest assemblage of atoms possible in which all the atoms are equivalent. It also has the largest possible number of point group symmetries (120). The history of the synthesis of C_{60} is also interesting from another point of view. The original discoverers, Kroto, Smalley *et al.*, were chemists by background but made use of physical techniques–cluster beam apparatus and time-of-flight mass measurement–to first observe the molecule [4]. But the practical bulk synthesis was devised by physicists, Krätschmer and Huffman [5], using extraction techniques taken directly from the chemistry laboratory. Thus one sees in the study of clusters a blurring of the distinctions between physics and chemistry. Once macroscopic quantities became available, it was possible to measure properties that would be extremely difficult otherwise. An example from the original paper is the infrared absorption spectrum, shown in Figure 2. Due the high symmetry of the molecule, there are only four optical active transitions, although the number of vibrations is much larger, $3N - 6 = 174$. We will come back to this spectrum in Section 4.

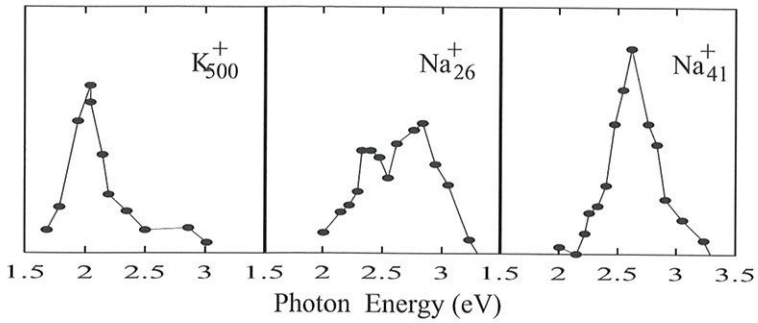

Fig. 3. Surface plasmon in alkali metals. Left, K_{500}^+ from reference [7]; middle and right $Na_{26,41}^+$ from reference [8].

There are many properties of clusters that can be measured in cluster beam experiments. The ionization potential can be measured rather directly in photoionization experiments from the threshold energy. The binding energy of an atom to the cluster is measured indirectly through the evaporation rate and its temperature dependence, using statistical theory. A recent example of the application of the theory to determine the atom separation energy in Na clusters may be found in [6].

The response of clusters to external electromagnetic fields is a large subject, and will be the main topic of my lectures. An external electric field $\mathcal{E}$ induces a dipole moment D; the linear polarizability α is the coefficient of proportionality in the expansion $D = \alpha\mathcal{E} + ...$ This is commonly measured by deflection of a beam in an inhomogeneous electric field. One can also study magnetic clusters by their deflection in an inhomogeneous magnetic field, the classic Stern–Gerlach experiment. Magnetic properties of clusters will be a topic in Pastor's lecture.

The photon absorption cross section is also measured over a frequency range starting from optical frequencies to the very far ultraviolet (~10 eV photon energy). In simple metal clusters one sees a coherence between the electrons in that there is strong peak in the response involving all of the valence electrons. This is the surface plasmon mode, and I shall have quite a bit to say about it. Figure 3 shows some typical optical absorption spectra of metal clusters. In a spherical cluster, the surface plasmon is sharply defined, as may be seen in the first panel, showing potassium spectra [7]. The plasmon is split in nonspherical clusters, as shown in the second panel. This geometric sensitivity of the plasmon may be understood at many levels, from classical to quantum mechanical. This feature of cluster behavior is

also reminiscent of a similar phenomenon in nuclear physics. I will show how an analytic rough description be derived looking at the short-time behavior of the wave function.

The main aim in these lectures is to give the student some familiarity with the basic tools the theorist has at his disposal to study these cluster properties, particularly electronic excitations. In this respect one should emphasize the importance of simple models. For describing large numbers of particles, the use of models that focus on a few degrees of freedom is unavoidable. Even if one's efforts are in large-scale *ab initio* numerical calculations, the models are extremely useful to interpret the numbers and check the numerics. My own cluster research, published in the papers [9–31], has evolved from applications of simple ideas taken from nuclear physics to numerically intensive computations of *ab initio* theory. While I will show some of these *ab initio* results that are won by intensive computer computation, I think one of their main values is to validate simpler models.

Before discussing electronic excitations, I will go through statistical reaction theory, which is indispensable to interpret cluster formation and evaporation, and many electron transfer processes.

2 Statistical reaction theory

An important tool for understanding dynamic processes in clusters, as well as for extracting information about their energetics, is statistical reaction theory. Like statistical mechanics, the theory is well-known in principle. But much of the literature is confusing, and I think it is worthwhile to assemble all the relevant formulas and their derivations. The generic problem is to calculate the emission rate of an excited state of a bound system. The derivation of the statistical rate formula is based on detailed balance, which is one of the fundamental principles of statistical mechanics. If we divide the system's phase space up into microstates, the equilibrium state has all the microstates equally occupied. Looking at the detailed dynamics, the probability flux out of each microstate must equal the probability flux in. The inward flux is relatively straightforward to compute or to characterize empirically. Then making the equality gives us a way to calculate the emission rate. Note that the emission rate does not depend on the system being in equilibrium with its surroundings. It only depends on there being equilibrium among the internal microstates of the system.

We sketch a system, Figure 4, with one degree of freedom singled out, say the position of the particle that will be emitted. All the other degrees of freedom will be treated by imagining the Hamiltonian to be diagonalized, and so represent them by states. In the scattering problem these states with a fixed radial coordinate for the particle are called channels. We now put the

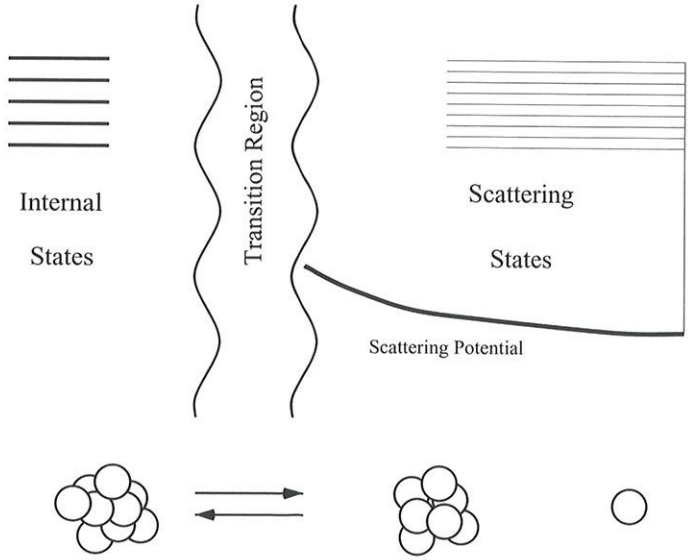

Fig. 4. Separation of internal and external states for the derivation of the statistical decay formula.

system in a box to make it easier to count states for the detailed balance argument. The thick curve in Figure 4 shows the energy of the lowest channel as a function of distance. The states of the system, separated into internal and external states, are shown with light lines. These are not the eigenstates of the system, because we have not coupled the internal to the external states. Let us now count the states and invoke detailed balance. For the external states, let us give the box a radius R. We will count the number of states in an energy interval ΔE, and we need the density of external states with respect to energy.

This is calculated as follows. For a large box, we can take the normalized asymptotic wave function to have the form[1]

$$\phi = \sqrt{\frac{2}{R}} \sin(k_n r),$$

[1]This ignores the scattering phase shift and the angular-momentum-dependent phase of the asymptotic wave function.

where n labels the different states. The density of the external levels $\mathrm{d}E/\mathrm{d}n$ is given by[2]

$$\frac{\mathrm{d}n}{\mathrm{d}E} = \frac{Rm}{\hbar^2 \pi k} .$$

Let us now find the inward current in an energy interval ΔE. The asymptotic external wave function has both incoming and outgoing components, with the incoming component given by

$$\phi = \sqrt{\frac{2}{R}} \frac{\mathrm{e}^{-ikr}}{2} .$$

The current associated with this component is

$$\langle j \rangle = -\frac{\hbar k}{4m} \frac{2}{R} .$$

When the particle reaches the cluster, it may be reflected immediately or it may be transmitted into the interior. Define the transmission coefficient T_c, with $0 \leq T_\mathrm{c} \leq 1$. Then the flux that goes into the target is the current of each state times the number of states times the occupation probability of each state. Calling the last quantity f_0, the inward flux is

$$f_0 T_\mathrm{c} \langle j \rangle \frac{\mathrm{d}n}{\mathrm{d}E} \Delta E = f_0 \frac{T_\mathrm{c}}{2\pi\hbar} \Delta E.$$

By detailed balance we can equate this to the outward flux, assuming that the internal states have the same occupation probability f_0. Let's define an average decay rate of an inner state, W. The total flux out is given by

$$f_0 W \rho_E \Delta E$$

where ρ_E is the density of internal states of the system. Equating the last two expressions gives the statistical formula for the decay rate W,

$$W = \frac{\sum_\mathrm{c} T_\mathrm{c}}{2\pi\hbar\rho_E} . \tag{2.1}$$

Note that the derivation does not require the system to be in equilibrium with its surrounding, only that there is an internal equilibrium among the internal states.

To use the formula, one needs to know the transmission coefficients as well as the level density of the internal states. In many applications the

[2]This may be derived from the boundary condition that the wave function vanish at the surface of the box[1], $k_n R = n\pi$, taking the asymptotic energy, $E = \hbar^2 k_n^2 / 2m$.

channel potential energy has a barrier, and one can make the approximation that the transmission coefficients are zero below the barrier and unity above. Then there is a correspondence between the channels and the level density of the daughter system. With these assumptions, one obtains the well-known transition state theory, called RRKM theory in chemistry. In principle the channels are discrete, and at energies close to the barrier energy the decay rate might show a step-like behavior. In fact, this was predicted in nuclear physics in the original fission theory of Bohr and Wheeler, which made use of equation (2.1). However, the discreteness of channels was never clearly seen in nuclear fission, because the quantum mechanical transmission coefficients increase smoothly as the channel opens. But in my last lecture I will show you an example from carbon structures that perfectly shows the individual channels.

The statistical decay formula also requires the density of states of the decaying system, ρ_E. Under ideal conditions when the internal states do not overlap, $(W < (\hbar\rho_E)^{-1})$, the internal states can be explicitly counted. This is the case in nuclear physics for energies close to the neutron emission barrier. For atomic clusters and molecules larger than several atoms, the vibrational density of states is huge compared to the electronic, and there is no hope to see individual internal states in the regime of electronic excitations.

2.1 *Cluster evaporation rates*

We now apply the formula to evaporation of atoms from a cluster. We consider a cluster having excitation energy E^*, emitting an atom of kinetic energy E_K and leaving the daughter cluster at excitation energy E_i. The energies are related by

$$E^* = E_i + E_K + D \tag{2.2}$$

where D is the binding energy of the atom to the cluster in the ground state. In general, the atom can be emitted in many angular momentum states, and each one will have its own channel. However, in the end the incoming flux is determined by the inverse reaction cross section. To derive a simple formula, let us assume that the atoms are spinless and that the specific state of the cluster play no role in the absorption cross section. Then the transmissions coefficients depend only on the orbital angular momentum l and the energy of the atom, and the reaction cross section is given by

$$\sigma_{\mathrm{r}} = \frac{\pi}{k^2} \sum_l (2l+1) T_l(E_K)$$

where $\hbar^2 k^2/2m = E_K$. Exactly the same sum will appear when one makes an approximate sum over channels in equation (2.1). The channel are distinguished by the internal state of the daughter cluster (including its angular momentum L), the orbital angular momentum of the evaporated atom l, and the total angular momentum of the system J. For a given initial state the total angular momentum is fixed, so the channel sum will involve sums over l and L. The conditions of evaporation are generally such that the maximum l is much less than the typical J. Then the channel sum over L can be enumerating with the familiar rules of angular momentum coupling, $L = J - l, J - l + 1, ..., J + l$, giving $2l + 1$ terms altogether. If the particle has spin with g states, the spin coupling increases the number of channels to $g(2l + 1)$. Then assuming that the internal states of the daughter are independent of L, the formula (2.1) can be expressed

$$W = \frac{g \sum_i \sum_l (2l+1) T_l}{2\pi\hbar\rho_E} \,. \tag{2.3}$$

Here the i sum is over internal states of the daughter for some typical angular momentum L. The transmission coefficient depends on the i only because the energy of the evaporated particle depends on how much energy is left in the daughter. We now replace the sum over l by the cross section formula, to get

$$W = \frac{g \sum_i k_i^2 \sigma_{\rm r}(E_K)}{2\pi^2\hbar\rho_E} = \frac{gm \sum_i E_K \sigma_{\rm r}(E_K)}{\pi^2\hbar^3\rho_E} \,. \tag{2.4}$$

Here the evaporated particles momentum k and kinetic energy E_K depend on i through equation (2.2). The differential decay rate with respect to E_K is easily obtained by the replacing the sum over internal states by their level density, $\mathrm{d}\Sigma_i/\mathrm{d}E \to \rho_E$. The formula is,

$$\frac{\mathrm{d}W}{\mathrm{d}E_K} = \frac{gm\rho_{N-1}(E^* - D - E_K) E_K \sigma_{\rm r}(E_K)}{\pi^2\hbar^3\rho_N(E^*)} \,. \tag{2.5}$$

Here we have changed notation on the level density ρ to distinguish the parent density ρ_N and the daughter density ρ_{N-1} by a subscript. This formula was first derived by Weisskopf to describe neutron decay of excited nuclei [32].

Further reduction of this rate formula requires some specific information about the level densities. One simple limit is to assume that the excitation energy and level densities are high enough that the level density of the daughter system behaves exponentially over the range of the interest in the decay. This permits a parameterization with a temperature: $\rho_N(E^* - D - E_K) \approx \rho_N(E^* - D)\exp(-E_K/T)$, and equation (2.5) can be integrated with

respect to E_K. If we further assume that the cross section is constant, the integral is elementary and the total transition rate becomes[3]

$$W = \frac{mT^2 \rho_{N-1}(E^* - D)\sigma_r}{\pi^2 \hbar^3 \rho_N(E^*)} .$$

We now specialize to level densities associated with vibrations. If the vibrations are harmonic, the level density can be expressed completely analytically by Kassel's formula [33],

$$\rho_N(E) = \frac{E^{s-1}}{(s-1)! \prod_j^s (\hbar\omega_j)} . \tag{2.6}$$

Here s is the number of vibrational degrees of freedom, with $s = 3N - 6$ for triatomic and larger clusters. The sum goes over the vibrations j with their frequencies ω_j. Since the formula will be derived in Wales' lectures, I need not discuss its validity here.

Again assuming that the reaction cross section is constant, we can integrate over the density of states of the daughter system to get the following formula

$$W = \frac{\omega^3}{\pi^2}(s-1)m\sigma_r \frac{(E^* - D)^{s-2}}{(E^*)^{s-1}} . \tag{2.7}$$

Here ω^3 is the ratio of the products of vibrational frequencies for parent and daughter. The decay rate in essentially this form was originally derived by Engelking [34]. Note that the quantum of action $\hbar$ has dropped out of the formula. Once one takes Kassel's density of states, the remaining physics is completely classical.

For midsize and larger clusters there are many vibrational degrees of freedom, $s \gg 1$. It also usually the case that the evaporation is observed in a regime with $E^* \gg D$. Then the conditions for an exponential approximation are satisfied, and we can write $(E^* - D)^{s-2}/(E^*)^{s-2} \approx \exp(-D/T)$ where T is defined $T = E^*/(s-2)$. Note that the relation between T and E^* is exactly what one obtains classically for the relation between temperature and energy in a system of $s - 2$ oscillators. The decay rate formula then becomes

$$W = \frac{\omega^3 m\sigma_r}{\pi^2 T} \mathrm{e}^{-D/T} . \tag{2.8}$$

The most important feature of this formula is the extreme dependence of the evaporation rate on D. Let us take the example of sodium cluster of

[3] We have also assumed that the spin of the particle can be neglected ($g = 1$).

size $N \approx 100$. The binding energy of an atom is about $D \approx 1$ eV, and we will approximation ω by the Debye frequency, $\hbar\omega \approx 0.01$ eV. Let us also assume that T in the range of values near room temperature, $T = 0.025$ eV, to evaluate the prefactor in the formula. Although equation (2.8) does not have $\hbar$ in it, it is convenient to express frequencies as equivalent energies. Two more needed dimensional constants: $\hbar = 0.658$ eV-fs is needed to get a decay rate in units of s^{-1}, The mass is conveniently expressed in terms of $\hbar^2/m_{\rm H} = 4.15 \times 10^{-3}$ eV-Å^2. The inverse cross section is estimated as $\sigma_{\rm r} = \pi R^2 \approx 300$ Å, that is, assuming that all atoms that hit the cluster will stick. Putting the numbers together, we find

$$W \approx \frac{(0.01)^3(23)(300)}{\pi^2(0.00415)(0.025)} {\rm e}^{-D/T} \approx 10^{16} {\rm e}^{-D/T}.$$

Cluster beams have flight times of the order of tens to hundreds of microseconds. Thus a measurable evaporation rate requires the exponential suppression factor to be in the range $\exp(-D/T) \approx 10^{-11}$, *i.e.* $D \approx 25T$. We can see from this that a 10% change in D will change W by an order of magnitude. For $T = 0.03$ eV, the excitation energy is $E^* = 9$ eV, and the evaporation leaves the daughter clusters at the energy $E \approx 8$ eV. Thus, the chain of evaporations has very different rates for each stage, and the multiple evaporation spectrum will be very much peaked around the number that corresponds to a lifetime equal to the travel time in the cluster beam. As you will see, Haberland will use this property to accurately measure energy differences between clusters at different temperatures.

2.2 *Electron emission*

The statistical theory of electron emission is no different in principle, but there can be important differences in the details. Because of the Coulomb interaction, the geometric area may no longer be a good approximation to the reaction cross section.

Haberland will discuss in his lectures measurements of the electron emission in sodium clusters. He will show a very interesting result that the emission takes place when the electrons have equilibrated among themselves but before the equilibration with the vibrations has taken place.

Under these conditions, the state densities in equation (2.5) should be evaluated for the electron degrees of freedom only. The Fermion character of the electrons has two consequences. The two spin degrees of freedom gives rise to an additional factor of 2 in the formula, because there are twice as many external electron states when detailed balance is applied. Also, the level densities are quite different for Fermions. If we assume that the particles behave as a free Fermi gas, the level density has an exponential

dependence on excitation energy given by Bethe's formula,

$$\rho_E \sim \exp\left(2\sqrt{\pi^2 NE/2E_{\mathrm{F}}}\right),$$

where E_{F} is the Fermi energy of the electron gas. It is interesting to note that in the Fermion case the quantum effects remain visible in the final formula as the factors of $\hbar$ no longer cancel.

A final difference is that the inverse cross section cannot be considered constant, due to the long-range Coulomb interaction between the electron and the (charged) daughter system. The semiclassical formula for the cross section when there is complete absorption at a radius R in the present of a potential field V is

$$\sigma_a b = \pi R^2 \left(1 - \frac{V(R)}{E}\right).$$

Note that this diverges at low energy when the Coulomb potential is attractive. The divergence is only apparent, because the cross section is multiplied by E in the rate formula. This theory of charged particle emission is well known in nuclear theory; it was first applied to clusters in reference [35].

2.3 Radiative cooling

The last process I will discuss is the statistical emission of a photon. To observe radiative cooling in isolated clusters, one needs longer residence times than is provided by the usual molecular beam apparatus. Observations have been reported using ion traps [36] and storage rings [37]. In these experiments, the photons were not observed directly, but rather the effect of the cooling on other processes was seen. Also, it is interesting to note that cluster radiation was proposed as a way to achieve more efficient thermal illumination [38]. We will see that in the spectrum infrared emission is suppressed compared to black body radiation. In the derivation of the photon decay rate, only the transmission factor in the dipole channel ($l = 1$) is significant, but the formula looks very similar to equation (2.3). Photons have two polarization states, making $g = 2$. Also the energy of the photon E_{ph} and the reduced wave number k are related by $k = E_{\mathrm{ph}}/\hbar c$, so the final result for The result for the radiation spectrum is

$$\frac{\mathrm{d}W}{\mathrm{d}E_{\mathrm{ph}}} = \frac{1}{\pi^2}\frac{{E_{\mathrm{ph}}}^2}{\hbar c}\sigma_{\mathrm{r}}\frac{\rho_E(E^* - E_{\mathrm{ph}})}{\rho_E(E^*)}. \tag{2.9}$$

This formula is also well-known in nuclear physics where radiative decays of hot nuclei have been studied for some time. In the cluster context, the formula was first derived in reference [39].

3 Optical properties of small particles

In the remainder of my lectures I will mainly discuss the theory of electronic excitations, but before getting into the equations to be solved, I will list for future reference a number of useful formulas for describing the electromagnetic properties of small particles. Here by small, I mean the wavelength is much larger than the size of the particle, $\lambda \gg R$. Then the electric dipole field dominates the interaction, and the optical response can be described with the dynamic polarizability $\alpha(\omega)$. For a spherical system, the polarizability is defined

$$\alpha_{zz}(\omega) = \frac{e^2}{\hbar} \sum_i |\langle 0|z|i\rangle|^2 \left(\frac{1}{-\omega - i\eta + \omega_i} + \frac{1}{\omega + i\eta + \omega_i} \right), \tag{3.1}$$

with i labeling excited states. For nonspherical systems, one can define polarizabilities for the principle axes and construct a polarizability tensor.

The photon absorption cross section is related to the polarizability by

$$\sigma_{ab} = \frac{4\pi\omega}{c} \mathrm{Im}\alpha(\omega). \tag{3.2}$$

An important property of the dipole response is the Thomas–Reiche–Kuhn sum rule. It may be derived from the operator commutator relation, $[z,[H,z]/2 = \hbar^2/2m_\mathrm{e}$. In terms of dipole matrix elements between ground and excited states i, the sum rule reads

$$\sum_i |\langle 0|z|i\rangle|^2 \hbar\omega_i = \frac{\hbar^2}{2m_\mathrm{e}} N, \tag{3.3}$$

where N is the number of electrons. Conventionally one defines a dimensionless oscillator strength f_i for a transition as

$$f_i = \frac{2m}{\hbar^2} |\langle 0|\, z\, |i\rangle|^2 \hbar\omega_i.$$

Then the sum rule is simply $\sum_i f_i = N$. In terms of the dynamic polarizability, an oscillator strength function can be defined

$$S_f(\omega) = \frac{2m_\mathrm{e}\omega}{\pi\hbar e^2} \mathrm{Im}\alpha(\omega) \tag{3.4}$$

and the f-sum is

$$\int \mathrm{d}\hbar\omega S_f(\omega) = f. \tag{3.5}$$

Another handy formula is the expression for f in terms of the integral of the cross section over the photon energy,

$$f = \frac{m_e c}{2\pi^2 e^2 \hbar} \int \sigma_{ab} \mathrm{d}E. \tag{3.6}$$

A practical formula used by chemists takes for the integrand the molar extinction coefficient rather that the cross section; a derivation may be found in my book [18].

3.1 Connections to the bulk

With clusters viewed as a bridge between the atom and the bulk, it is interesting to see how the electronic response connects to the infinite medium response. There the response is characterized by the dielectric function ϵ, which gives the relation between external and internal electric fields at a perpendicular interface: $\epsilon = \mathcal{E}_{\mathrm{int}}/\mathcal{E}_{\mathrm{ext}}$. There are two connections one can make to the finite system polarizability α. The first is the dielectric function for an cubic crystal composed of polarizable particles, given by the Clausius-Mossotti relation,

$$\epsilon = \frac{1 + 8\pi\alpha n_0/3}{1 - 4\pi\alpha n_0/3} = \frac{1 + 2\alpha/r_0^3}{1 - \alpha/r_0^3} \tag{3.7}$$

where n_0 is the number density of the particles in the crystal. For convenience in the second equation the formula is expressed in terms of the Wigner-Seitz radius r_0. This is the radius of a sphere whose volume corresponds to the volume per particle in the medium, $4\pi r_0^3/3 = 1/n_0$. A similar length r_s is in common use to specify the electron density n_e. This is defined $4\pi r_s^3/3 = 1/n_e$ and is quoted in atomic units (lengths in Bohr radii (0.529 Å); energies in Hartrees (27.2 eV).

The other connection is the polarizability of a cluster considered as a dielectric sphere. It is a textbook exercise in electrostatics to show that the polarizability of a dielectric sphere of radius R is given by

$$\alpha = R^3 \frac{\epsilon - 1}{\epsilon + 2} \cdot \tag{3.8}$$

We shall call this the Mie theory of the polarizability. One more handy formula is the dielectric function of a simple conductor. In the Drude model (independent electrons subject to a frictional force depending linearly on velocity) the dielectric function is

$$\epsilon(\omega) = 1 - \frac{\omega_p^2}{\omega(\omega + i\gamma)} \tag{3.9}$$

where γ is the frictional rate constant and $\omega_{\rm p}$ is the plasmon frequency,

$$\omega_{\rm p}^2 = \frac{4\pi e^2 n_{\rm e}}{m_{\rm e}} \cdot \tag{3.10}$$

In atomic units the formula is simply $\omega_{\rm p}^2 = 3/r_{\rm s}^3$.

Let us try this in equation (3.8). After some trivial algebra one finds

$$\alpha(\omega) = R^3 \frac{\omega_{\rm p}^2/3}{-\omega^2 + i\omega\gamma + \omega_{\rm p}^2/3} \cdot \tag{3.11}$$

There are two obvious things to notice about this formula. The first is that the zero-frequency limit gives $\alpha = R^3$, which is just the formula for the polarizability of a conducting sphere. The second is that there is a resonance where the denominator vanishes, near the frequency

$$\omega_{\rm s} = \frac{\omega_{\rm p}}{\sqrt{3}} = \sqrt{\frac{e^2}{m r_{\rm s}^3}} \cdot \tag{3.12}$$

This is the surface plasmon, and we shall call equation (3.12) the surface plasmon formula. In atomic units it is simply $\omega_{\rm s} = r_{\rm s}^{-3/2}$.

3.2 Linear response and short-time behavior

The photon absorption cross section and the polarizability are properties that only require the dynamics in weak external fields, the linear response region. This allows a variety of methods to be applied to solve the time-dependent equations, and each method has its adherents. There are two very popular methods that I will not describe in any detail in these written notes, but they need to be mentioned for completeness. In these methods one makes a matrix representation of the problem and either inverts or diagonalizes the matrix. Both methods start by Fourier transforming the Kohn-Sham equations in time, to obtain equations in the frequency domain. In the linear response region, different frequency are not coupled together except that the amplitude for a given frequency is coupled to that of its negative.

The direct solution of the time-dependent equations is possible, and I have pursued this method with my collaborator, Kazuhiro Yabana, using an algorithm originally developed for nuclear physics [40]. With the time-dependent equations, one can apply an external field of arbitrary shape and strength. If the field is weak, the response of a given frequency is obtained from the amplitude of that Fourier component in the excitation field. It is very convenient to take the perturbing field to be a δ-function in time,

because it has all Fourier components with equal weight. Let us first see how this works with the one-particle Schrödinger equation,

$$H\phi \equiv -\frac{\nabla^2\phi}{2m} + U(r)\phi = i\frac{\partial\phi}{\partial t}\cdot$$

Here $U(r)$ is a fixed internal potential the system. In this section I have dropped factors of $\hbar$ to simplify the formulas. I start with the ground state $\phi_0 \exp(-iE_0 t)$ and add to the Hamiltonian an impulsive external potential, $V_{\rm ext}(r,t) = V_0(r)\delta(t)$. The differential equation then requires that there be a corresponding jump in the wave function at $t = 0_+$,

$$\phi(0_+) = (1 - iV_0)\,\phi_0.$$

The subsequent evolution can be found by solving the equation as a power series in time. The form of the power series is

$$\phi(t) = \left(1 - iV_0 - [H, V_0]t + i[H,[H,V_0]]t^2/2 + \ldots\right)\phi_0 \mathrm{e}^{-iE_0 t}. \qquad (3.13)$$

The low-order terms in this expansion have direct physical interpretation in classical Newtonian mechanics. The initial perturbation of the wave function gives it the same momentum density that one would calculate from an impulsive force field $\vec{\nabla}V_{\rm ext}$ acting on a density distribution of classical particles. This may be seen from the expansion of the expression for the momentum density to linear order in the external field,

$$\vec{p}(r) \equiv \phi^*(0_+)\left(\frac{\vec{\nabla} - \overleftarrow{\nabla}}{2i}\right)\phi(0_+) = -\vec{\nabla}V_0|\phi_0|^2. \qquad (3.14)$$

Here the right hand side is just the momentum density associated with the force field $\vec{\nabla}V_{\rm ext}$ and the ordinary density $n_0 = |\phi_0|^2$. Next let us look at how the density varies in time. To first order in t the time-dependent density is given by

$$n(t) \equiv |\phi(t)|^2 = |\phi_0|^2 - 2\phi_0^*[H, V_0]\phi_0 t + \ldots = n_0 - \frac{\vec{\nabla}\cdot}{m} n_0 \vec{\nabla}V_0 t + \ldots$$

Taking the derivative of this expression to get $\partial n/\partial t$, and comparing with equation (3.14), one can recognize the equation of continuity

$$\frac{\partial n}{\partial t} = -\vec{\nabla}\cdot\vec{p}(r)/m = -\vec{\nabla}\cdot\vec{j}$$

where $\vec{j}(r) \equiv \vec{p}(r)/m$ is the particle current. The next term in the power series will give the initial change in momentum due to the internal forces

in the system. It is rather complicated to work out the double commutator for the next term in general (but see [9]), so I will specialize to the very importance case of the dipole field, $V_0 = \lambda z$. Here λ is a small parameter to remind ourselves that the response is to be calculated to linear order in the external field. The relevant commutators are

$$[H, V_0] = -\frac{\lambda}{m}\frac{\partial}{\partial z} \tag{3.15}$$
$$[H, [H, V_0]] = \frac{\lambda}{m}\frac{\partial U}{\partial z}\cdot$$

Inserting in equation (3.13), the wave function evolves as

$$\phi(t) = \left(1 - i\lambda z + i\frac{\lambda t^2}{2m}\frac{\partial U}{\partial z}\right)\phi_0 \mathrm{e}^{-iE_0 t} + \frac{\lambda}{m}\frac{\partial \phi_0}{\partial z} t\mathrm{e}^{-iE_0 t} + \ldots$$

The generalization of this expansion to a many-particle Hamiltonian with interactions between the particles is very similar. Let us consider the Hamiltonian $H = \sum_i p^2/2m + \sum_i U(r_i) + \sum_{i<j} v(r_i - r_j)$ and call the ground state wave function Ψ_0. Then the power series expansion of the wave function is

$$\Psi(t) = \left(1 - i\lambda t^2 \sum_i z_i + i\frac{\lambda}{2m}\sum_i \frac{\partial U(r_i)}{\partial z_i}\right)\Psi_0 \mathrm{e}^{-iE_0 t}$$
$$+ \frac{\lambda}{m}\sum_i \frac{\partial \Psi_0}{z} t\mathrm{e}^{-iE_0 t} + \ldots$$

Note that the last term in parentheses only contains the one-particle potential U. The particle-particle interaction does not contribute because the relevant commutator vanishes,

$$\left[v(r_i - r_j), \frac{\partial}{\partial z_i} + \frac{\partial}{\partial z_j}\right] = 0.$$

I next write down the power series expansion of the dipole moment and the total momentum. With a little bit of algebra, these quantities can be expressed as follows

$$D(t) \equiv \langle \Psi(t)|z|\Psi(t)\rangle = \lambda\frac{N}{m}t + \ldots \tag{3.16}$$

and

$$\langle \vec{p}\rangle \equiv \langle \Psi(t)|p_z|\Psi(t)\rangle = \frac{\lambda}{m}\left(N - \int \mathrm{d}^3 r n(r)\frac{\mathrm{d}^2 U}{\mathrm{d}z^2}t^2 + \ldots\right). \tag{3.17}$$

It is easy to connect this time-dependent analysis with the dynamic polarizability function considered at the begin of the section. Formally, we can expand the time-dependent wave function following the impulsive dipole field in the eigenfunctions,

$$\Psi(t) = \Psi_0 - i\lambda \sum_i \Psi_i \langle 0|z|i\rangle \mathrm{e}^{-i\omega_i t}.$$

The dipole moment and the total momentum then have the following time dependencies,

$$D(t) = \langle \Psi(t)|z|\Psi(t)\rangle = \lambda \sum_i 2\left|\langle 0|z|i\rangle\right|^2 \sin\omega_i t \tag{3.18}$$

$$\langle \Psi|p_z|\Psi\rangle = \lambda \sum_i 2\langle 0|p_z|i\rangle\langle i|z|0\rangle \cos\omega_i t. \tag{3.19}$$

In a power series expansion, the first term of the dipole moment is

$$\lambda \sum_f 2\omega_i \langle 0|z|i\rangle^2 t.$$

Comparing with equation (3.16), we see that they are equal if the TRK sum rule is satisfied. Thus the sum rule is just a statement about the short-time behavior of the wave function in an impulsive external field.

3.3 *Collective excitations*

It is possible to derive simple formulas for collective excitations just using the dynamics that was derived in the last section. From equation (3.19) we see that the power series expansion of the momentum has the first terms

$$\langle \Psi|p_z|\Psi\rangle = \lambda \left(N - t^2 \sum_i \omega_i^2 \langle 0|z|i\rangle\langle i|p_z|0\rangle + \ldots \right).$$

We can use this to estimate the frequency of the excitation, if the system is very collective. That assumption would allow us to replace the sum over states in the above equation by a single state with an excitation energy I will call ω_c. Comparing with equation (3.17), we find

$$\omega_c^2 = \frac{1}{mN} \int \mathrm{d}^3 r n(r) \frac{\partial^2 U}{\partial z^2}. \tag{3.20}$$

This formula can be used to make simple estimates of collective frequencies.

Let us first consider the spherical jellium model. The background charge density is $n_0\Theta(R-r)$ and the corresponding potential is

$$U = -\frac{4\pi e^2 n_0 R^3}{3r}, \quad r > R$$
$$U = -\frac{4\pi e^2 n_0 R^2}{3}\left(\frac{3}{2} - \frac{r^2}{2R^2}\right), \quad r < R.$$

If the electrons are contained within the jellium sphere, the integral in equation (3.20) reduces to $\int_0^R \mathrm{d}^3 r n(r) = N$ and we immediately get the surface plasmon formula, equation (3.12). We thus see a condition of validity of the formula: the electrons must be contained within the jellium sphere radius. In fact the electron wave functions will spill out, decreasing the integral and thereby the frequency of the collective oscillation.

A simple extension of the model allows us to derive a formula for the splitting of the surface plasmon frequency in deformed systems. Let us suppose we have a small quadrupolar deformation with the radius vector depending on direction according to

$$R(\theta) = R(1 + \beta P_2(\cos\theta))$$

where P_2 is the Legendre function and β is a dimensionless deformation parameter. Taking β small, the charge density distortion of the jellium background is approximately

$$\delta n = \beta R n_0 P_2(\cos\theta)\delta(r - R).$$

The Coulomb potential associated with this charge density be obtained from the multipole expansion. The result for $r < R$ is

$$\delta U = -\beta \frac{4\pi e^2 n_0 r^2}{5} P_2(\cos\theta).$$

The mode in the x or y direction will now have a different frequency from the z mode because the respective second derivatives of the field $U + \delta U$ differ. Working this out, we get to leading order in β

$$\omega_{\mathrm{s}}^x = \omega_{\mathrm{s}}^y = \omega_{\mathrm{s}}\,(1 + 3\beta/5)$$
$$\omega_{\mathrm{s}}^z = \omega_{\mathrm{s}}\,(1 - 6\beta/5)\,.$$

4 Calculating the electron wave function

From a computational point of view, it is extremely difficult to calculate many-particle wave functions for more than a few particles, because the

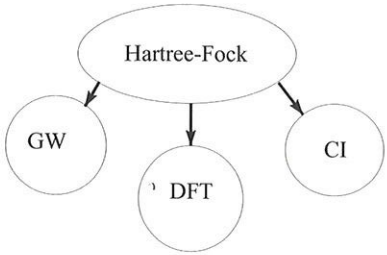

Fig. 5. Hierarchy of quantum many-body theories.

number of functional values needed in a numerical representation increases exponentially with the number of independent variables. On the other hand, the calculation of single-electron wave functions in an arbitrary three-dimensional potential is within the scope of desktop computers. Fortunately, there is a theory that is quite accurate although it only involves the solving the one-particle Schroedinger equation.

The most sophisticated version of the theory is called the time-dependent density functional theory or TDDFT for short. I will show a number of calculations done with TDDFT, but before that it is useful to review the static theory. This is the density functional theory (DFT). For systems larger than a few atoms, it has revolutionized the computation of electronic properties, as indeed was recognized in the 1998 Nobel Prize. While it has been spectacularly successful in calculating static properties, it does have well-known deficiencies in treating excitations. It is therefore important to understand the approximations and their validity.

The kinds of theory one can make for electronic structure are shown in Figure 5. In my view, Hartree–Fock theory is fundamental to all proven approaches. The theory is very simple to describe: minimize the expectation of the Hamiltonian in the space of Slater determinants. You have seen the basic objects many times before:

$$\Psi = \mathcal{A}\prod_i \phi_i(r_i), \quad \langle\phi_i|\phi_j\rangle = \delta_{ij} \tag{4.1}$$

$$E = \langle\Psi|H|\Psi\rangle = \sum_i \int \mathrm{d}^3 r \frac{|\vec{\nabla}\phi_i|^2}{2m} + \int \mathrm{d}^3\, r n_\mathrm{e}(r) V_\mathrm{ion}(r) + \frac{e^2}{2}\int \mathrm{d}^3 r \mathrm{d}^3\, r' \frac{n_\mathrm{e}(r) n_\mathrm{e}(r')}{|r-r'|} - \sum_{i<j}\left\langle \phi_i\phi_j \left| \frac{e^2}{|\vec{r}-\vec{r}'|}\right| \phi_j\phi_i \right\rangle \tag{4.2}$$

where $n_\mathrm{e}(r) = \sum_i |\phi_i(r)|^2$ is the electron density. The variation $\delta E/\delta\phi_i^*(r) = 0$ gives the Hartree–Fock equations. The single-particle energy

Table 1. Atomization energies.

	Li_2	C_2H_2	20 simple molecules (mean absolute error)
Experimental	1.04 eV	17.6 eV	-
Theoretical errors:			
Hartree–Fock	−0.94	−4.9	3.1
LDA	−0.05	2.4	1.4
GGA	−0.2	0.4	0.35
τ	−0.05	−0.2	0.13

in the Hartree–Fock equations arises as a Lagrange multiplier to preserve the norm of the wave function. While Hartree–Fock is conceptually simple, on a practical level it is not accurate enough to be useful for chemistry or for computing cluster structures. The level of accuracy for several simple molecules is shown in Table 1, taken from Perdew [41, 42]. The mean absolute error in the atomization energies (energy difference between the molecule and the individual atoms in isolation) is 3 eV in the Hartree–Fock theory. The predicted binding of the Li_2 clusters is a factor ten too low, and another alkali metal cluster not in the table, Na_2, is incorrectly predicted to be unbound.

The three lines in Figure 5 going down from Hartree-Fock give three different approaches to improve the theory. The "CI", configuration interaction expansion, uses Hartree-Fock as a basis of many-body wave functions. This is a very systematic approach, and it gets marvelous results in small systems, as you will see in the seminar of Bonačič-Koutecky. But the number of terms needed in the CI expansion to achieve a given accuracy grows exponentially with the number of electrons. So one turns to other methods to deal with larger systems.

Many-body perturbation theory was developed in the 1950's to make possible systematic calculation of the energy of quantum systems with an infinite number of particles. One avoids the many-body wave function, but the price one pays is to deal with Green's functions that depend on a few more variables. In condensed matter physics, the most refined approximation that can be presently computed this way is called the "GW" approximation. You can find a review of it by Hedin [43]; I will not discuss it here in any detail.

The last approach to make a better theory is to keep the form of the Hartree–Fock equations, but improve the energy function that is put into the variational principle. The DFT will thus include effects of correlations

by changing the Hamiltonian. In practice, there is another aspect of DFT as it is normally applied, the local density approximation (LDA). Evaluation of the exchange interaction is computationally burdensome, and approximations to make it look like an ordinary potential have been used since the time of Slater. In defining the effective exchange potential, one is guided by the energies in the uniform electron gas. The exchange energy of an electron of momentum k is [44]

$$-\sum_i \left\langle ki \left| \frac{e^2}{|r-r'|} \right| ik \right\rangle = -\frac{e^2 k_\mathrm{F}}{\pi} \left(1 + \frac{k_\mathrm{F}^2 - k^2}{2kk_\mathrm{F}} \log \left| \frac{k+k_\mathrm{F}}{k_\mathrm{F}-k} \right| \right), \tag{4.3}$$

where k_F is the Fermi momentum. The total exchange energy (per electron) E_x is given by

$$E_\mathrm{x} = -\sum_{i<j} \left\langle ij \left| \frac{e^2}{|r-r'|} \right| ji \right\rangle = \frac{-3}{4\pi} e^2 k_\mathrm{F} = \frac{-3}{4\pi} e^2 (3\pi^2 n_\mathrm{e})^{1/3}$$

where in the last equation we used the relation between electron density n_e and Fermi momentum, $n_\mathrm{e} = k_\mathrm{F}^3/3\pi^2$. Slater proposed making a local density approximation by using a two-body contact interaction that would have the same total energy. The one-body potential in the Schrödinger equation would then be

$$V_\mathrm{Slater}(r) = -\frac{3}{2\pi} e^2 (3\pi^2 n_\mathrm{e}(r))^{1/3}.$$

THIS IS WRONG. Going back to the variational principle, one sees that the one-body potential should be defined by the variation of E_x,

$$V_\mathrm{x}(r) = \frac{\delta n E_\mathrm{x}}{\delta n} = -\frac{e^2}{\pi} (3\pi^2 n_\mathrm{e}(r))^{1/3}. \tag{4.4}$$

This is a factor 2/3 different from Slater's potential.

Kohn and Sham proposed to include the correlation energy of the electron gas in exactly the same way, determining an exchange-correlation potential V_xc from the exchange-correlation energy E_xc of the interacting Fermi gas. This is usually done through a numerical parameterization, giving us the "LDA" of density functional theory. It gives a considerable improvement over Hartree–Fock, as may be seen by the entries in Table 1. However, the accuracy is still not enough for chemical modeling. An obvious problem of the LDA is that the single-particle potential does not have the correct asymptotic behavior. The electron potential in a neutral cluster should behave as $-e^2/r$ for large separation of the electron from the cluster. But in the LDA the Coulomb potential is calculated with all the electrons and thus

Table 2. Atomic properties of the Ag atom in LDA.

	IP	First excitation
Experimental	7.75	3.74
Kohn–Sham:		
eigenvalues	$\epsilon_s = 4.6$	$\Delta\epsilon = 3.9$
total energies	8.0	4.1

vanishes outside the cluster. This makes the LDA unreliable for calculating ionization potentials from the Kohn-Sham eigenvalues.

As an example of the last problem, Table 2 shows the ionization potential (IP) of the silver atom and the excitation energy of its first excited state. According to Hartree–Fock theory, the Ag atom has a single electron in a s orbital, with an unoccupied p orbital just above and a fully occupied d orbital just below. Thus the IP should correspond to the energy of the s-orbital. For the silver atom, the Kohn–Sham eigenvalue is off by 40% from the experimental ionization potential. Nevertheless the LDA can give quite accurate ionization potentials if they are calculated a different way, namely as a difference of total energies,

$$IP = E(\mathrm{Ag}) - E(\mathrm{Ag}^+). \tag{4.5}$$

The table shows that the error is only 3% when the IP is calculated this way. For the excitation energy, which is an $s \rightarrow p$ transition, the difference of Kohn–Sham energies $\Delta\epsilon = \epsilon_p - \epsilon_s$ is fairly good. However, there are caveats that we will come back to later.

Becke [45] proposed a fix to get the $-e^2/r$ asymptotic potential by adding a term to the energy functional that depends on the gradient of the density, $\nabla n_{\mathrm{e}}(r)$. His proposed form works amazingly well. This is the "generalized gradient approximation", GGA. From Table 1, we see that energies can be calculated to an accuracy of tenths of an eV. Further improvements may be possible. The Kohn–Sham energy functional depends on the nonlocal quantity

$$\tau = \sum_i |\nabla\phi_i|^2$$

in the kinetic energy term. One could think of using other functional dependencies on τ; an example is given in the last line of Table 1.

Before going on to electronic excitations, I want to show how well the LDA works for describing the infrared active vibrations in C_{60}. One first calculates the LDA potential energy surface as a function of displacement

Table 3. Excitation energies of C_{60} infrared-active vibrations (T_{1u}).

Mode	1	2	3	4
Experimental	0.065 eV	0.071	0.147	0.177
LDA error				
Ref. [22]	−2%	−2%	+2%	+10%
Ref. [46]	−3%	−7%	−8%	−7%

of the atoms from their ground state positions. Diagonalizing the Hessian matrix then gives the normal modes and their frequencies. The results of three different LDA calculations are shown in Table 3. The agreement with experiment is impressive, with mean absolute relative error on frequency only 4%. A more demanding test of the theory is the transition strength associated with the vibrations. The accuracy here is perhaps only a factor of two [22]. But that is a great improvement over previous theories that were completely unreliable.

4.1 Time-dependent density functional theory

Schrödinger proposed two equations in his original paper, the eigenvalue equation for static properties and the time-dependent equation for the dynamics. But the left-hand side of both equations was the same. The situation is the same for dynamic theories based on Hartree–Fock or DFT. The theories may be derived from the time-dependent variational principle,

$$\delta \int \mathrm{d}t \left\langle \Psi \left| H - i\frac{\partial}{\partial t} \right| \Psi \right\rangle = 0. \tag{4.6}$$

Taking Ψ to be a Slater determinant, and varying with respect to $\phi_i^*(r)$, one obtains time-dependent Hartree–Fock equations, first proposed by Dirac in 1930. The corresponding equations for DFT are the time-dependent Kohn–Sham equations,

$$-\frac{\hbar^2}{2m_\mathrm{e}}\nabla^2\phi_i(r,t) + \left(\int \mathrm{d}^3r' \frac{e^2 n(r,t)}{|r-r'|} + V_\mathrm{xc}[n(r,t)] + \sum_\mathrm{ions} V_\mathrm{ion}(r-R_\mathrm{I}) \right) \phi_i(r,t) = i\hbar\frac{\partial}{\partial t}\phi_i(r,t). \tag{4.7}$$

The first application of TDDFT was to describe the photoionization of atoms [47]. The theory has since been widely applied to clusters, molecules,

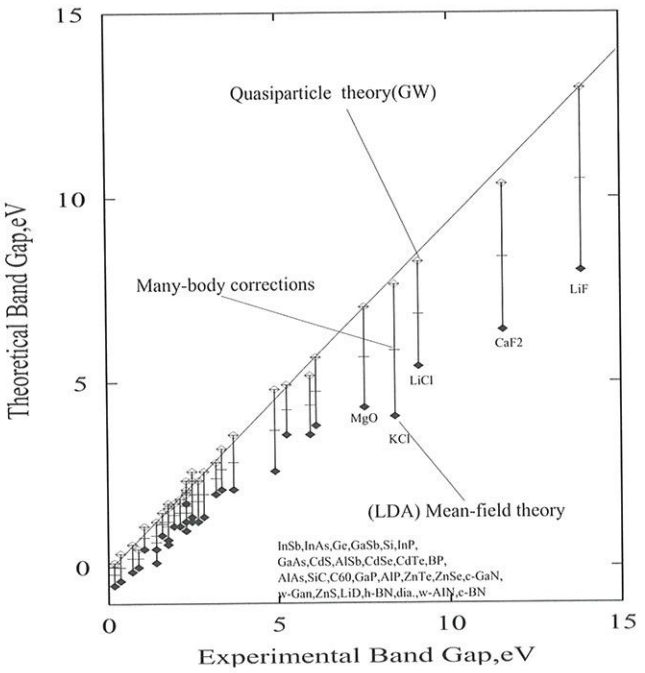

Fig. 6. Band gap in insulators and semiconductors, theoretical *versus* experimental for the GW approximation and for the DFT. From Hedin [43].

and bulk matter. There are several quite different methods to solve the equations, which I will not discuss in detail.

Before describing the applications to clusters, I want to give a cautionary remark. It is tempting to apply DFT to excitations by simply replacing the ground state single-particle wave functions by excited state orbitals in the Kohn–Sham equation. This seems to work well for small systems, as for example in the Ag atom discussed earlier, and in small carbon structures that will be discussed later. However, the theory can give poor results in large systems. This is the "band gap" problem. This may be seen in Figure 6 showing the band gaps between occupied and unoccupied bands in some insulators and semiconductors. The DFT, shown with black diamonds, is consistently low, by as much as 5 eV in the LiF crystal.

The band-gap problem originates in the LDA treatment of exchange. From equation (4.3) one sees that the exchange potential of an electron in a Fermi gas has a weak logarithmic singularity at the Fermi surface. Particle-hole excitations across the Fermi surface have a higher energy for a given

momentum difference than the quadratic kinetic energy functional. Because the singularity is weak, it does not show up for small systems. Clearly, any local approximation will miss the singularity. An effective, but computationally costly method to overcome this is to calculate the electron energies from the many-body perturbation theory. In the GW approximation, the electron-self energy is calculated including exact exchange. The GW theory gives an enormous improvement to the band gap, as may be seen from Figure 6. But the computational demands of the theory has so far restricted its application to relatively simple systems.

5 Linear response of simple metal clusters

In this section I want to present some results for metal clusters. The most simple are the alkali metals, having only a single valence electron in the s-atomic orbitals. The jellium model, introduced in Section 3 and to be discussed in detail by Manninen, describes the qualitative properties of sodium clusters very well. The metals in the IB column of the periodic table (the "coinage" metals Cu, Ag, Au) also have a single valence electron in the s-orbital, but in these metals there is a filled d-shell just below the valence shell, which affects the properties quite strongly. We shall first discuss the alkalis and then see the differences with the IB metals.

5.1 Alkali metal clusters

At the crudest level, the optical response of the metals will show a surface plasmon at a frequency given by the surface plasmon formula equation (3.12). If we take the density n_e at the bulk value for sodium, the formula gives

$$\omega_s \approx 3.4 \text{ eV}.$$

In fact, the observed surface plasmon is at a lower frequency ("red-shifted"). For example, the optical absorption spectrum of the cluster Na_{41}^+ in Figure 3 shows the resonance at a frequency of 2.6 eV. One possibility to explain the red shift would be that the density of atoms in the cluster is less than in the bulk. This idea is not born out in DFT calculations of the cluster structure, so I will not discuss this possibility any further. Another mechanism to explain the red shift is the spillout of the electrons, as mentioned in Section 3. We can analyze this mechanism quantitatively by calculating the optical response of the jellium model. There is a computer code, called JellyRpa, that I wrote and distributed [11] to calculate the response of spherical jellium, making no other approximations on the dynamics. Indeed there is an effect of the spillout, as may be seen in Figure 7. The peak is shifted from

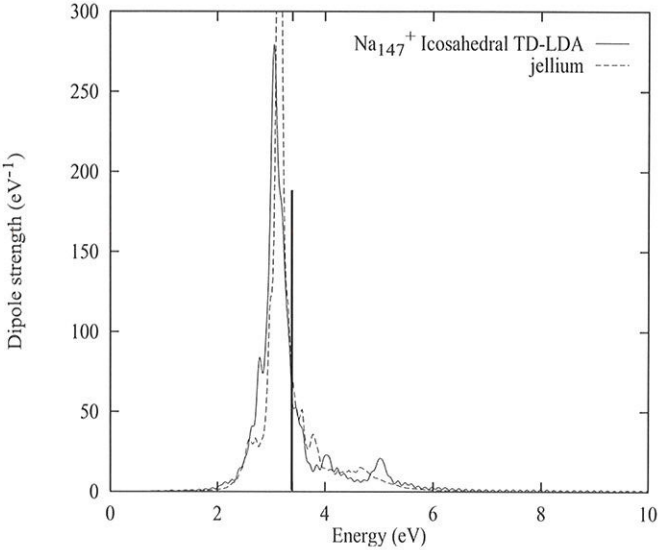

Fig. 7. Comparison of jellium model of a large sodium cluster with the surface plasmon formula and the TDDFT. The transition from the surface plasmon formula is shown with a vertical line.

3.4 to 3.0 eV, which is about half of what is needed to explain the empirical position. Another possibility is that the local density approximation might not be accurate enough. In particular, we saw in Figure 6 that the local approximation to exchange could produce serious errors in infinite systems. This question was addressed in finite clusters by Madjet *et al.* [48], who examined and compared the different treatments of exchange. They found that the LDA exchange was quite satisfactory for sodium clusters, and could not be the reason for the discrepancy.

Lastly, the jellium approximation might be inadequate; the full TDDFT of course includes a realistic treatment of the ionic potentials. Comparing the full TDDFT with the jellium, we found mixed results. Taking the ionic potential from the naive pseudopotential prescriptions in the literature, we found a surface plasmon at the same frequency as in the jellium model. This is also shown in the figure. However, there is an different prescription for the pseudopotential [49], treating the core electrons somewhat differently. This gives an additional red shift, essentially bringing the surface plasmon down to the observed position. In the end, it is rather disquieting that a seemingly small change in the ionic potential would have a very noticeable effect on the absorption spectrum.

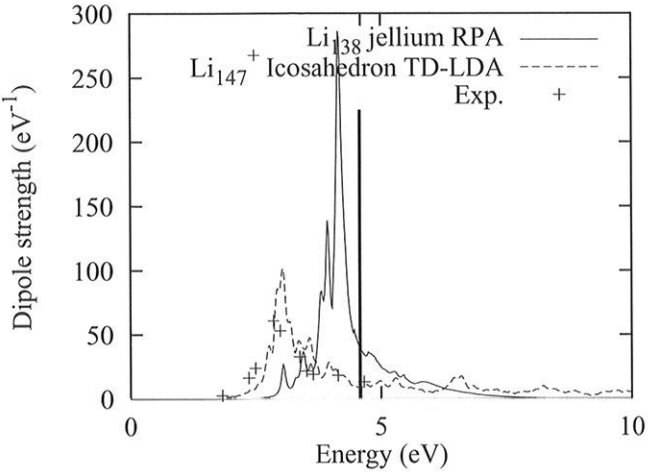

Fig. 8. Surface plasmon in Li clusters with $N \approx 150$. The prediction from equation (3.12) is shown by the vertical line.

There is an even larger red shift in lithium clusters: the formula gives 4.6 eV, while the observed peak in the absorption spectrum is at 3.0 eV [51]. Here it is much easier to understand how the shift arises from the ionic potential. The ionic potential is different for s and p waves because there is a core s orbital that is excluded from the valence wave function but no corresponding excluded p state. Thus, the ionic potential is effectively more attractive for p orbitals. This makes it easier to excite the electrons from the ground state, and lowers the excited state energies. This can be seen in Figure 8, comparing the jellium model with the full TDDFT calculation. As well as substantially shifting the peak position, the TDDFT disperses the strength somewhat on the high-frequency side. Both features are seen in the experimental data, which is rather well reproduced by the TDDFT.

The strength of the surface plasmon in sodium clusters, both theoretically and experimentally, is very close collective limit with f equal to the number of valence electrons. In lithium clusters, the effect of the ionic potential may be interpreted as a giving the electron an effective mass $m^* \approx 1.3m$, which also reduces the sum rule by the same factor (*e.g.* see [50]).

5.2 Silver clusters

The surface plasmon formula is also poor for silver clusters, but for a different reason. Here the formula gives 5.4 eV, but the observed surface plasmon

is in the range 3.5–4.0 eV. In this case, it is not justified to neglect the polarization of other electrons, namely the filled d-shell [52]. In reference [28] we calculated spectra of silver clusters including explicitly the d-electrons in the TDDFT. The observed peaks in Ag_8, for example, are nicely reproduced by the theory. In Ag_9^+ the experimental spectrum [53] shows a single peak at 4 eV, having a width of about 1 eV. The theory gives several transitions in the range 3.6–4.4 eV that together could give a single broad peak of about the needed width. Thus the theory reproduces the energetics of the surface plasmon rather well.

I now want to show the role of the d-polarizability in the properties of the plasmon from a more analytic point of view. I start with description of the polarizability of the d-electrons in the Ag atom. This somewhat unphysical quantity was calculated in [28] by the TDDFT keeping the s-electron frozen as the ground state orbital. The polarizability of the core came out to be $\alpha_d \approx 2$ Å$^3 \approx 14$ a.u. at the surface plasmon frequency. In that work we derived the effect on the surface plasmon using the linear response technique. Here I will show another derivation using the dielectric function. We can associate a dielectric function with the d polarizability using the Clausius–Mossotti formula, equation (3.7), $\epsilon_d = (1 + 2\alpha_d/r_0^3)/(1 - \alpha_d/r_0^3)$. For silver $r_0 = r_s = 3.02$, giving $\epsilon_d \approx 4$. Thus the d-orbital polarizability screens external fields by a considerably factor.

Let us redo the dielectric theory of the response including separate contributions from the s- and the d-orbitals. To derive the dielectric function for mixed sets of charges, we go back to the definition of the dielectric function and the relation to surface charges. There will be two surface charges screening the field, σ_d and σ_s. In terms of the internal field $\mathcal{E}_{\rm int}$ inside the conductor, the surface charges are given by

$$4\pi\sigma_{s,d} = (\epsilon_{s,d} - 1)\mathcal{E}_{\rm int}.$$

The same equation also holds for the total charge and total dielectric function, so one can easily derive for the complete dielectric function

$$\epsilon = \epsilon_d + \epsilon_s - 1.$$

Taking ϵ_d from the Clausius–Mossotti formula and ϵ_s from the free electron model equation (3.9) the dielectric function becomes

$$\epsilon = \frac{1 + 2\alpha_d/r_0^3}{1 - \alpha_d/r_0^3} - \frac{\omega_p^2}{\omega(\omega + i\gamma}\,. \tag{5.1}$$

Next we put this into the Mie formula for the polarizability. With a bit a algebra the expression becomes (dropping the $i\gamma$)

$$\alpha = R^3\frac{1-\epsilon}{2+\epsilon} = R^3\frac{\omega_s^2(1 - \alpha_d/r_0^3) - \omega^2\alpha_d/r_0^3}{\omega_s^2(1 - \alpha_d/r_0^3) - \omega^2}\,. \tag{5.2}$$

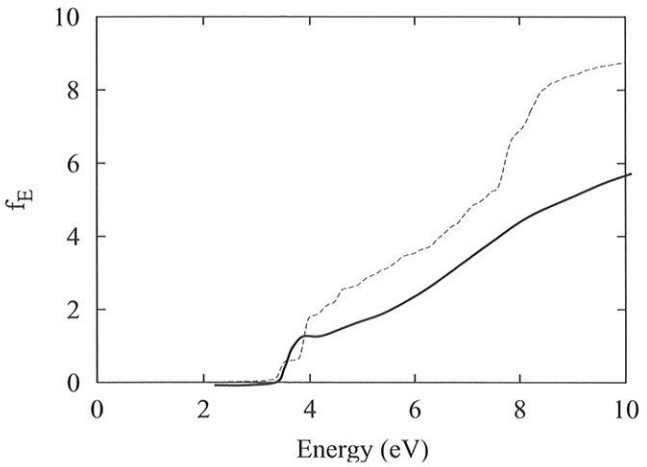

Fig. 9. Integrated strength function in Ag_8 comparing Mie theory (solid line) with TDDFT (dashed line).

From the denominator one sees immediately that the resonance energy is shifted to

$$\omega_s' = \omega_s(1 - \alpha_d/r_0^3)^{1/2}.$$

Taking the previous numerical value for ϵ_d, this gives $\omega = 3.7$ eV, which is almost exactly what is needed to describe the empirical resonance. In effect, the charges of the s-electrons are screened by a factor $\sqrt{1 - \alpha_d/r_0^3}$.

I finally want to discuss the strength of the surface plasmon. Unlike the alkali metal clusters, the strength is strongly reduced by the d-electron screening, at least in theory. Figure 9 shows the integrated strength function, $f_E = \int_0^E \mathrm{d}E' S(E')$ for Ag_8, calculated in the TDDFT and in the Mie theory using the empirical dielectric constant for silver metal. The two curves are surprisingly similar. Thus with respect to the theoretical polarizability, a small silver cluster seems to behave as a piece of the bulk metal. In the Mie theory, the surface plasmon is seen as the step at 3.6 eV. The finite system calculation gives a split peak, with the stronger excitation slightly blue-shifted. The height of the step gives strength of the resonance; we see that it is roughly 2, which is a factor of 4 lower than the number of valence s-electrons in the clusters. This another manifestation of the screening by the d-electrons. It can also be understood rather simply by the above polarizability function. In the neighborhood of the resonance,

the above polarizability can be expressed

$$\alpha \approx \frac{R^3}{2}\omega_s'(1-\alpha_d/r_0^3)\left(\frac{P}{\omega-\omega_s'}+i\pi\delta(\omega-\omega_s')\right).$$

Putting this in equation (3.4), we find for the associated strength,

$$f = N(1-\alpha_d/r_0^3)^2.$$

Since the coupling to the external field goes as e^2, each charge here is screened by a factor $1-\alpha_d/r_0^3$. Numerically, the predicted screening is a factor of 4, as found in the microscopic calculation.

The situation would be completely satisfactory except that it does not agree with experiment. The experiment of Tiggesbäumker *et al.* [53] measured not only the position of the resonance in Ag_9^+ but also its strength. The integrated strength over the resonance is about 4, more than twice the theoretical value. I am sorry that I can not give you a resolution of this disagreement. But the measurement of total strength is not easy experimentally, and so one should not give up the theory without additional confirmation.

6 Carbon structures

In this lecture I will discuss carbon structures, going from small clusters and molecules to fullerenes and nanotubes. A very simple theory, the Hückel model, turns out to be an excellent guide to the electronic structure obtained by more elaborate means such as the density functional theory. There are two requirements for the Hückel model to be applicable. The first is that each carbon and its neighbors lie in a plane. Then the symmetry with respect to plane allows the orbitals to separated into σ or π types having even or odd reflection symmetry, respectively. This classification is in fact useful even if the planar condition is not strictly met, as in the curved fullerenes and nanotubes. The other condition is that the π orbitals are at the Fermi surface. This is the case for all the systems I consider. The π orbitals on different atoms couple rather weakly, and the Hückel models treats the wave function by the amplitude of the π orbital on each carbon, constructing the eigenstates from the simple hopping Hamiltonian

$$H = -\beta\sum_{s}^{2}\sum_{j_1,j_2} a_{j_1 s}^{\dagger}a_{j_2 s}.$$

Here the sum j_1, j_2 runs over pairs of adjacent carbon atoms, s is a spin label, and β is a parameter giving the hopping matrix element between the

atoms. The hopping parameter can depend on distance d between carbon atoms when that varies. It will turn out that a fair parameterization is given by [29]

$$\beta(d) = 2.5 \left(\frac{1.40 \text{ Å}}{d} \right)^{2.7} \text{ eV}. \tag{6.1}$$

6.1 Chains

The first structures I want to consider are linear chains. If the axis of the chain is in the z-direction, both the p_x and p_y atomic orbitals will have π character. To find the spectrum within the Hückel model, we start with an infinite system. Here, by the Bloch theorem, the eigenfunctions have amplitudes on the atoms that vary from atom to atom as exponentials:

$$\phi_K(j) \sim \exp(ijK) \tag{6.2}$$

where K is a parameter of the eigenstate and j indexes the atom in the chain. Then ϕ_K is the solution of the Hamiltonian equation

$$H\phi_K = \epsilon_K \phi_K$$

with energy

$$\epsilon_K = -2\beta \cos K. \tag{6.3}$$

To find the solution for a finite chain, I use a trick. Namely, the wave function on a finite chain with N atoms at positions $j = 1, 2, ..., N$ behaves the same under the hopping Hamiltonian as a wave function on an infinite chain, provides the wave function vanishes at sites 0 and $N + 1$. There is no hopping from these sites in the finite system because there are no atoms there. The vanishing boundary conditions are satisfied by sine functions with parameters $K = \pi m/(N + 1)$, where m is an integer. The normalized wave functions are then

$$\phi_m(j) = \sqrt{\frac{2}{N+1}} \sin \frac{\pi m j}{N+1} \quad m = 1, 2, ...$$

From equation (6.2) the energies of the orbitals are

$$\epsilon_m = -2\beta \cos \left(\frac{\pi m}{N+1} \right). \tag{6.4}$$

Let's see how well this compares with the LDA energies. In Figure 10 we compare the Kohn–Sham energies of the π orbitals in the cluster C_7 with

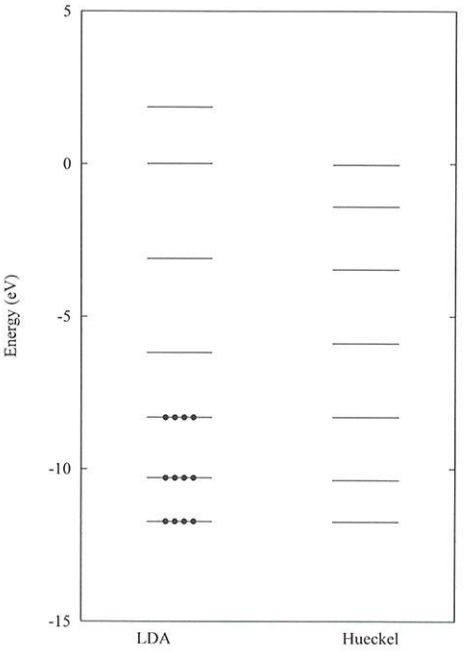

Fig. 10. Comparison of π orbital energies in the C_7 cluster.

equations (1.2–3). The hopping parameter in the Hückel model was taken from equation (6.1) and energy scale was set by aligning the highest occupied orbital, $m = 3$. The occupied orbitals are indicated by black circles in the figure. We see that the Hückel model is quite accurate in the neighborhood of the Fermi energy and below.

A very important derived property is the gap between occupied and unoccupied orbitals. For odd-numbered chains, the highest occupied orbital has $m = (N-1)/2$. Thus the gap energy is

$$\Delta\epsilon = 2\beta\left(\cos\frac{(N-1)\pi}{2(N+1)} - \cos\frac{(N+1)\pi}{2(N+1)}\right) = 2\beta\sin\frac{\pi}{N+1}\cdot \tag{6.5}$$

Asymptotically, the gap for large chains decreases as

$$\Delta\epsilon \sim \frac{1}{N}\cdot \tag{6.6}$$

The comparison of LDA [25] with the Hückel model as function of chain size is shown in Figure 11. There is one complication that shows up as an odd-even staggering in the LDA spectrum. The π orbitals in a chain have a

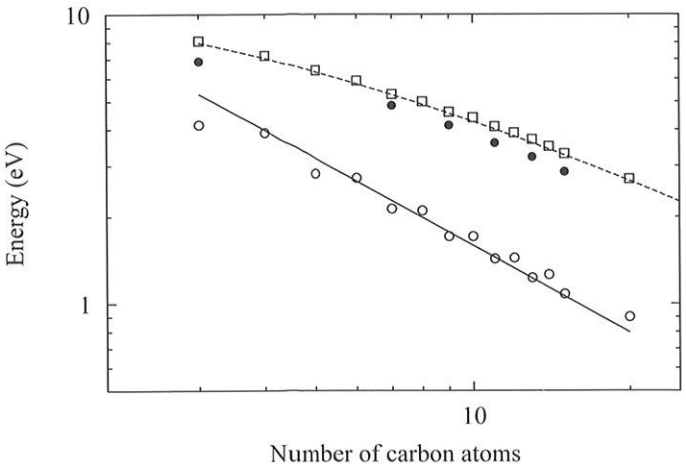

Fig. 11. Systematics of the energy gap and the collective excitation in carbon chains, compared with functional fits of the form (6.6) and (6.10). The filled circles show the experimental energies of transitions of clusters in a noble gas matrix, from references [54, 55].

two-fold spatial degeneracy (as well as the usual two-fold spin degeneracy). The highest occupied orbital is only half filled for even N, giving them a different gap.

The excitation of an electron from just below to just above the Fermi level will have a large transition strength, close to the number of electrons in the π manifold of states. Under these conditions, the frequency of the excitation will be strongly perturbed from the gap energy $\Delta\epsilon$. When the TDDFT is applied, the Coulomb interaction pushes the strength to higher energy. Of course the total strength is preserved due to the Thomas–Reiche–Kuhn sum rule.

The TDDFT calculated energies of the strong transitions are show as the boxes in Figure 11. The shift from the gap energy is factor of 2–3, making the transition very collective. The theory describes the experimental data (shown by filled circles) quite well. Note that experimental data is only available for the more stable odd-number clusters. A ring structure is probably more preferable in the midsize even-number clusters.

A qualitative description of the transition energies can be obtained using the matrix version of the TDDFT theory and considering only the single state, the excitation across the gap $\Delta\epsilon$. The matrix version of TDDFT

reduces to a simple formula in that case, giving a transition energy ω

$$\omega = \sqrt{\Delta\epsilon(\Delta\epsilon + 2v)}. \tag{6.7}$$

This formula is the same as equation (4.12) in reference [18], which contains a derivation. To find the interaction v, let us assume that it depends only on the distance between carbon atoms and has the following form

$$\begin{aligned} v(j_1, j_2) &= U \quad j1 = j2 \\ &= \frac{e^2}{d|j_1 - j_2|} \quad j1 \neq j2 \end{aligned} \tag{6.8}$$

where d is the distance between carbon atoms. The matrix element for an excitation from orbital m_1 to m_2 is then

$$v = 4 \sum_{j_1, j_2} \phi_{m_1}(j_1)\phi_{m_2}(j_1)\phi_{m_1}(j_2)\phi_{m_2}(j_2)v(j_1, j_2)$$

with the factor 4 coming from the degeneracy of the orbitals. Taking the two coefficients in equation (6.8) as parameters, the TDDFT calculations shown in the figure are fit with parameter values $e^2/d = 11.7$ eV and $U = 11.7$ eV. The value for e^2/d is very close to what one would expect from the distance between carbons, $d = 1.28$ Å. Note also that the on-site interaction U is not stronger than the interaction between neighboring carbons. The reason is that the exchange and correlation energies compensate the stronger onsite Coulomb interaction.

It is interesting to examine the asymptotic behavior of ω for large chains. We already found that $\Delta\epsilon$ has an $1/N$ behavior but v has a different dependence. With the form equation (6.8) for the interaction, and the sum over pairs has an asymptotic logarithmic dependence on N coming from the $1/|j_1 - j_2|$ term. The logarithmic dependence was noted in [25] and compared with an analytic formula analytic formula derived from the plasmon dispersion in a long wire,

$$\omega^2 = \frac{4\pi n e^2 q^2}{m_e} \log \frac{1}{qa} \cdot \tag{6.9}$$

Here a is the radius of the wire, and q is the wave number. For a finite chain, we may take $q \sim 1/N$, and the N-dependence of the excitation becomes

$$\omega = \frac{\sqrt{A + B \ln N}}{N} \cdot \tag{6.10}$$

One see in Figure 11 that a straight line (corresponding to $1/N$ in the logarithmic plot) gives a good fit to the N-dependence for $\Delta\epsilon$ but not for ω. The wire formula other hand describes the N-dependence of ω quite well.

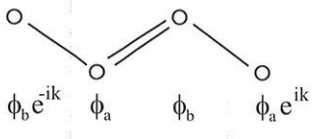

Fig. 12. Hückel wave function construction for polyacetylene.

6.2 Polyenes

The next system I will discuss are chain molecules have alternating single and double bonds between the carbons, the conjugated carbon molecules. These are the polyene molecules, beginning with the two-carbon molecule ethylene and going to the infinite chain, polyacetylene. The molecules have hydrogen atoms as well, which do not play any role in the π orbitals. As before, it is easier to solve the Hückel Hamiltonian for the infinite system. In the polyenes, the distance between the carbons alternates, depending on whether the bond is single or double. Thus there will be two hopping matrix elements, β_s and β_d. To solve the problem, we divide the chain into unit cells containing two carbon atoms attached by a double bond. The system is periodic with this unit cell so we can write the wave function for the atoms in the cell and adjacent to the cell as shown in Figure 12.

Let us apply the Hamiltonian equation $H\phi = \epsilon\phi$ at two sites in the unit cell. This gives the two equations,

$$\begin{aligned} -\beta_s\phi_b e^{-iK} - \beta_d\phi_b &= \epsilon\phi_a \\ -\beta_d\phi_a - \beta_s\phi_a e^{iK} &= \epsilon\phi_b. \end{aligned} \tag{6.11}$$

The equations are easily solved (multiplying them together) to get a formula for the energy,

$$\epsilon_k = \pm\sqrt{\beta_s^2 + \beta_d^2 + 2\beta_s\beta_d \cos K}. \tag{6.12}$$

Interestingly, it has a gap at half filling given by

$$\Delta\epsilon = 2|\beta_d - \beta_s|. \tag{6.13}$$

In this case I don't know a trick to get the finite system spectrum from this result. But the Hückel Hamiltonian is easy to diagonalize numerically, with the dimensionality of the matrix equal to the number of carbon atoms. Fitting the LDA energies of the 8-carbon polyene, one finds hopping parameters of 2.27 and 2.80 eV. These parameterization fits the LDA energy

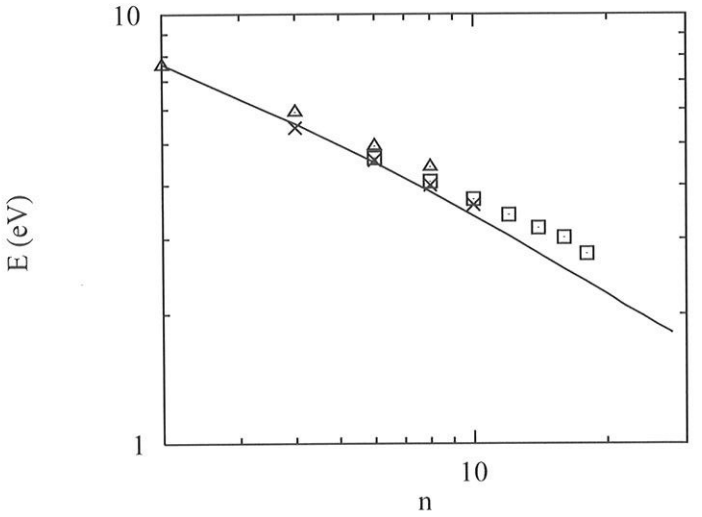

Fig. 13. Transition energy of the collective $\pi - \pi^*$ transition in polyenes, comparing theory with experiment. The TDDFT is the solid line; the points are various experimental measurements. See reference [29] for details.

gap of all of the polyenes in the range $N = 2{-}40$ very well. However, in polyacetylene, the predicted gap from equation (6.13) is 1.08 eV, which is rather far off the experimental value of 2.1 eV. This is undoubtedly the same gap problem of extended insulators that was mentioned in Section 2. The problem is seen in the LDA calculations of very large finite polyenes [56]. As in the case of the semiconductors, the GW approximation gives a much better gap [57].

Let us now examine the excitation energies of the strong transitions. The results of the TDDFT are compared with experimental data in Figure 13. The agreement is rather satisfactory. It would be interesting to analyze these results in the framework of the Hückel model, but I have not done so.

6.3 Benzene

We now turn to the benzene molecule, which for the Hückel molecule is a perfect hexagon of carbons (bond length 1.40 Å); the outside hydrogens hardly affect the π electrons. I will analyze the orbitals with a poor man's group theory, utilizing only the 6-fold rotation symmetry about the center of the hexagon. We can still make use the wave function from equation (6.2), but now the boundary condition is that $\phi_K(0) = \phi_K(6)$, giving $K = m\pi/3$

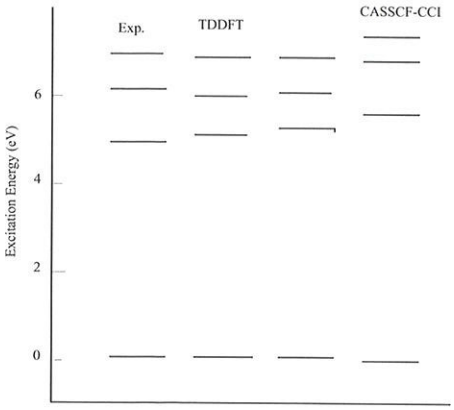

Fig. 14. Singlet $\pi - \pi^*$ vertical excitation energies of benzene.

for integers m. Here m has the same meaning as the azimuthal quantum number of the rotation group. The wave functions and orbital energies are then given by

$$\phi_m(j) = \frac{1}{\sqrt{6}} \mathrm{e}^{imj}$$
$$\epsilon_m = -2\beta \cos \frac{m\pi}{3} \cdot \tag{6.14}$$

The lowest state has $m = 0$, and then there are two degenerate states with $m = \pm 1$. The 6 π electrons in benzene fill these three orbitals (with each orbital containing two spin states). The lowest unoccupied orbital is the two-fold degenerate $m = \pm 2$ pair. The sixth and highest orbital has $m = \pm 3$. The state is the same for either sign of m. The energy gap is given simply by $\epsilon_2 - \epsilon_1 = 2\beta$.

Four distinct excitations can be made at the energy gap, due to the degeneracies of the orbitals just above and below the gap. The particle-hole states can be labeled by the change in m required to produce the state. For example, the $M = +3$ state has the electron in orbital $m = -1$ promoted to the orbital $m = +2$. Thus it appears that there should be two two-fold degenerate excitations, $M = \pm 1$ states and $M = \pm 3$ states. The former are have dipole matrix elements with the ground state and will be prominent in optical absorption spectrum. The latter two states mix together, due to the indistinctness of the ± 3 transition density. This gives an energy splitting between the states, leading to a spectrum with three excitation energies.

Figure 14 shows this energetics, and compares with the full scale time-dependent density functional theory. The uppermost state ("$^1E_{1u}$") has a large optical absorption transition strength, and can be described as a

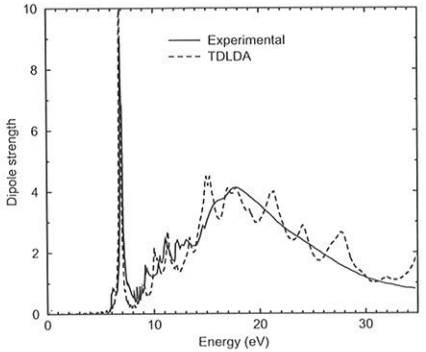

Fig. 15. Comparison of experimental and theoretical absorption spectrum in benzene, from reference [29].

$\Delta M = \pm 1$ transition. The next state down is weaker by a factor of ten, and is assigned the linear combination $|+3\rangle + |-3\rangle$ of the $\Delta M = \pm 3$ transitions. The other linear combination, $|+3\rangle - |-3\rangle$, has vanishing transition density on the carbon atoms, and is hardly shifted by the interaction from the unperturbed excitation energy $\Delta\epsilon$. The TDDFT theory gives an excellent account of these states with no free parameters. In the Hückel theory, we already get the lowest state because it is at the gap energy. It is interesting to see how well a simple Hückel model does for the energy shifts of the other states. Taking the Hückel model for the wave functions in the E_{1u} excitation, the matrix element for the $(m = 1) \rightarrow (m = 2)$ excitation is

$$v = \frac{1}{3}(v(0,0) + v(0,1) - v(0,2) - v(0,3)).$$

Taking $v(0,0)$ from Section 6.1 and the others as $v(0,j) = e^2/r_{ij}$, the matrix element is 3.6 eV and equation (6.7) gives an excitation energy of 7.6 eV, compared to 7.0 eV experimentally. So in this case the simple formula is somewhat inaccurate.

As one goes higher in energy, there are many more states that can be excited, and the TDDFT gives a prediction for the entire spectrum. The absorption spectrum is shown in Figure 15, compared with the TDDFT theory. As stated above, the sharp state at 7.0 is the collective $\pi - \pi^*$ transition. Just above, there is some tiny structure in the experimental spectrum that reminds one of tuft of grass. These are the so-called Rydberg states, having a very loosely bound electron in the Coulomb field of the ion. These states cannot be described in the LDA because of its incorrect

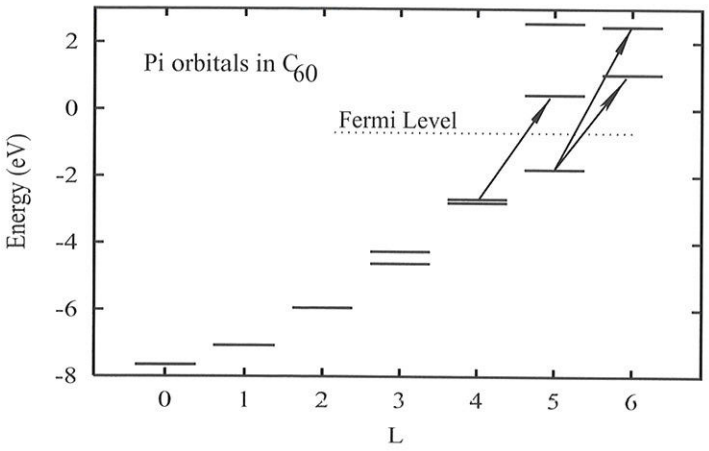

Fig. 16. Comparison of π orbital energies in the C_{60} molecule.

asymptotic potential field. The broad structure centered around 15 eV is due to the more tightly bound σ electrons. Its center position and overall width is correctly described by the theory. However, one can see that the theory has additional structure at high energy while the experimental cross section is very smooth. This is probably an artifact of the numerical method used to calculate the TDDFT, placing the system in a box.

6.4 C_{60}

The fullerenes are also carbon structures whose lowest excitations are contained in the $\pi - \pi^*$ manifold. The nearly spherical shape of C_{60} implies that angular momentum quantum numbers can be used to some extent to classify the orbitals. Thus, the lowest orbital of π character has an equal amplitude on all the carbon atoms, corresponding to $L = 0$. This classification breaks down at high L, where the discreteness of the Hückel Hamiltonian becomes visible in the spectrum. The spectrum of π orbitals is shown in Figure 16 with assigned L values. We see that the Fermi level splits the $L = 5$ orbitals. The arrows in the figure show the allowed $\pi - \pi^*$ transitions. The total transition strength occupied and empty π orbitals is about $f = 15$, which is considerably smaller than the number of π electrons (40). Experimentally, and in the TDDFT, one sees a group of transitions at about 7 eV excitation with a combined strength of about $f = 10$. Qualitatively, these transitions can be understood with the tight-binding model [12].

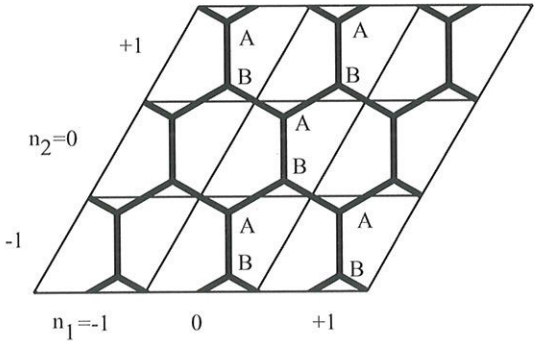

Fig. 17. Unit cells in the graphene lattice.

6.5 Carbon nanotubes

The last stop on my survey of carbon structures takes us up to extended nanostructures, the carbon nanotubes. They have very interesting electronic properties. Depending on their structure, they can be conductors or semiconductors, and one can even observe the individual conduction channels. Their properties may be understood with the Hückel model, at least on a qualitative level.

As we did before, we start with the theory for an infinite system, in this case an infinite graphite sheet. We follow the same route we used in constructing the wave functions for polyacetylene. Like polyacetylene, there are two atoms in the graphite unit cell (see Fig. 17). We label the two atoms "A" and "B" and distinguish the atomic amplitudes accordingly. Let us suppose we have an eigenstate, decomposed into A-site amplitudes $\phi_{\rm A}(n_1, n_2)$ and $\phi_{\rm B}(n_1, n_2)$ where (n_1, n_2) labels the cell in the two-dimensional lattice. Then the Hückel Hamiltonian only connects A and B amplitudes with each other,

$$\begin{pmatrix} 0 & H_{\rm AB} \\ H_{\rm AB} & 0 \end{pmatrix} \begin{pmatrix} \vec{\phi}_{\rm A} \\ \vec{\phi}_{\rm B} \end{pmatrix} = \epsilon \begin{pmatrix} \vec{\phi}_{\rm A} \\ \vec{\phi}_{\rm B} \end{pmatrix}. \tag{6.15}$$

From the structure of these equations it follows immediately that the spectrum of eigenvalues comes in pairs with equal and opposite sign. For each solution with energy ϵ we can get another state with energy $-\epsilon$ by the changing the sign of the $\phi_{\rm B}$'s while keeping $\phi_{\rm A}$ the same. This symmetry of the spectrum with respect to the sign of the energy was seen in benzene and polyacetylene and will be seen again in Manninen's lectures, and arises whenever the lattice can be divided into two equivalent sublattices with the Hamiltonian matrix elements zero within each sublattice.

We are particularly interested in the states at the Fermi level, which is at zero energy because of the half filling of a symmetric spectrum. So our task is now to determine the structure of wave functions of zero energy in the graphite lattice. There will be several of them, allowing arbitrary linear combinations of $\phi_{\rm A}$ and $\phi_{\rm B}$ on some particular unit cell. As an example we can assume that $\phi_{\rm B}(0,0) = 0$ and $\phi_{\rm A}(0,0) = 1$. We may also assume that the state is a Block wave, so we can characterize it with the vector $\vec{K}_{\rm F} = K_1^{\rm F}(\hat{x} - 1/\sqrt{3}\hat{y}) + K_2^{\rm F}(2\hat{y}/\sqrt{3})$ where the two components K_1, K_2 give the phase change moving a cell to the right and to the upper right, respectively. Thus

$$\phi_{\rm A,B}(n_1, n_2) = {\rm e}^{i(K_1 n_1 + K_2 n_2)}\phi_{\rm A,B}(0,0).$$

Then all $\phi_{\rm B}$ amplitudes are zero, and equation (6.15) is trivially satisfied. The other condition, $H\vec{\phi}_{\rm A} = 0$, reads as follows when expanded out for the B amplitude on the site (0,0):

$$-\beta\left(\phi_{\rm A}(1,-1) + \phi_{\rm A}(0,-1) + \phi_{\rm A}(0,0)\right) = \\ -\beta\left({\rm e}^{i(K_1^{\rm F} - K_2^{\rm F})} + {\rm e}^{-iK_2^{\rm F}} + 1\right)\phi_{\rm A}(0,0) = 0.$$

The only way to satisfy this equation is to have the three terms in the middle expression be the three cube roots of one; thus

$$(K_1^{\rm F}, K_2^{\rm F}) = \pi(2/3, 4/3) \text{ or } \pi(-2/3, -4/3). \tag{6.16}$$

Since there is no continuous degree of freedom left in the choice of $K_1^{\rm F}$ and $K_2^{\rm F}$, the Fermi surface is a set of isolated points. This is the well-known structure of the graphite Fermi surface: there is no energy gap between occupied and empty orbitals, but unlike a metal the Fermi surface has zero area. For other values of (K_1, K_2), the energy can be found the same way we used for polyacetylene. The result is

$$\epsilon(\vec{K}) = \pm\beta\sqrt{(1 + \cos(K_1 - K_2) + \cos K_2)^2 + (\sin(K_1 - K_2) - \sin K_2)^2}.$$

When $\vec{K} = K_1\hat{x} + K_2(\hat{x}/2 + \sqrt{3}\hat{y}/2)$is near a $\vec{K}_{\rm F}$, the result can be approximated as [59]

$$\epsilon(\vec{K}) \approx \frac{\sqrt{3}}{2}\beta|\vec{K} - \vec{K}_{\rm F}|. \tag{6.17}$$

We are now ready to look at nanotubes. We can construct a nanotube by rolling up a sheet of graphite, joining the sides so the hexagons align,

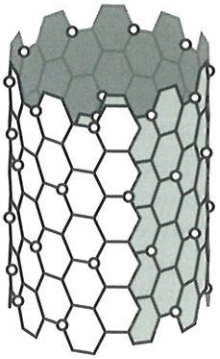

Fig. 18. Fermi surface on a carbon nanotube.

as shown in Figure 18. The various ways of aligning the hexagons can be distinguished by counting along the hexagons how far it is around the tube to come back to the starting hexagon. The counting is done along adjacent hexagons along the two directions corresponding to K_1, K_2 above.

Our $\epsilon = 0$ wave function will wrap around onto itself if the phases match on the superposed hexagon. This is the case for the tube in Figure 18, but will not be so if the hexagons are displaced one or two in any direction. The precise condition is

$$K_1 N_1 + K_2 N_2 = 2n\dot{\pi}$$

which from equation (6.16) is equivalent to

$$\mathrm{mod}(N_1 - N_2, 3) = 0.$$

If it is satisfied, there is a state at the Fermi energy and thus there is a conduction channel. If the condition is not satisfied, there is a gap at the Fermi surface and the conduction channels only open when the chemical potential is changed to put the Fermi level with the allowed states of the channel.

The density of states can be measured by scanning tunneling microscopy and one can see the higher states from the peaks at the thresholds (called Van Hove singularies) [60]. In the cited reference, the authors observed a number of peaks in a nanotube that they identified as a (13,7) structure, nearly symmetrically distributed about $\epsilon = 0$. The ones closest to the middle were at $\epsilon \approx \pm 0.9$ eV. To see whether this makes sense, let's put the boundary condition for a simpler tube, the (10,10), into equation (6.17). The extra state then appears when $10\Delta K_1 + 10\Delta K_2 = 2\pi$. Taking $\Delta K_1 = \Delta K_2$, the condition becomes $\Delta K_1 = \pi/10$; and the formula gives $\beta K_1 \approx (2.5)(\pi/10) \approx 0.78$ eV, which is rather close to the measured value.

6.6 Quantized conductance

The conductance of the individual channels can be derived from the statistical reaction theory with two assumptions. Let us attach the two ends of the nanotube to (electron) reservoirs and measure the current as a function of the Fermi levels of the two reservoirs. The first assumption is that the electrons travel through the tube independently. Then we can apply the statistical theory to the single-electron level densities. The next assumption is that the electrons go through without reflection and disappear into the other reservoir, *i.e.* the transmission coefficient of the channel is unity. It is then very easy to derive the formula for the conductance considered as a statistical emission of electron from each reservoir into the other. The formula is

$$I = n_{\mathrm{c}} \frac{e^2}{2\pi\hbar} V$$

where V is the potential difference of the two reservoirs in volts and n_{c} is the number of open channels, including the two spin states of the electron as two separate channels. I will not go through the details in these notes because the algebra is just the same as in my two-page published derivation in [12]. The staircase behavior of the above expression as the channels open up is seen in many conductance measures on nanoscale structures. An example of this phenomenon seen in the carbon nanotubes is [61]. This particular experiment seems to show a case where $n_{\mathrm{c}} = 1$, which can only be if one spin state of the electron is blocked. To my knowledge, there is no explanation for a strong spin dependent transmission.

Many of the results presented here were obtained in collaboration with K. Yabana, and his contribution is gratefully acknowledged. The author also thanks D. Tomanek for discussions related to Section 6.5, C. Guet for discussions related to Section 5, and T. Döppner and Q. Huang for proofreading the manuscript. The author's research mentioned in these lectures was supported by the Department of Energy under Grant FG06-90ER-40561.

References

[1] W.D. Knight *et al.*, *Phys. Rev. Lett.* **52** (1984) 2141.
[2] A.L. Mackay, *Acta Cryst.* **15** (1962) 916.
[3] O. Echt *et al.*, *Phys. Rev. Lett.* **47** (1981) 1122, Xe clusters.
[4] H.W. Kroto *et al.*, *Nature* **318** (1985) 163.
[5] W. Krätschmer *et al.*, *Nature* **347** (1990) 354.
[6] J. Borggreen *et al.*, *Phys. Rev. A* **62** (2000) 013202.
[7] C. Brechignac *et al.*, *Phys. Rev. Lett.* **68** (1992) 3916.
[8] J. Pedersen *et al.*, *Z. Phys. D* **26** (1993) 281.
[9] G. Bertsch and W. Ekardt, *Phys. Rev. B* **32** (1985) 7659.
[10] G.F. Bertsch and D. Tomanek, *Phys. Rev. B* **40** (1989) 2749.

[11] G. Bertsch, *Comp. Phys. Comm.* **60** (1990) 247. The program JELLYRPA may be downloaded from the author's Web site, `www.phys.washington.edu/~bertsch`
[12] G.F. Bertsch, N. Oberhofer and S. Stringari, *Z. Phys. D* **20** (1991) 123.
[13] G.F. Bertsch, *J. Phys. Cond. Matt.* **3** (1991) 373.
[14] G. Bertsch, A. Bulgac, D. Tomanek and Y. Wang, *Phys. Rev. Lett.* **67** (1991) 2690.
[15] K. Yabana and G. Bertsch, *Chem. Phys. Lett.* **197** (1992) 32.
[16] Y. Wang, C. Lewenkopf, D. Tomanek and G. Bertsch, *Chem. Phys. Lett.* **205** (1993) 521.
[17] Y. Wang, G. Bertsch and K. Ieki, *Zeit. Physik D* **25** (1993) 181.
[18] G.F. Bertsch and R.A. Broglia, *Oscillations in Finite Quantum Systems* (Cambridge Univ. Press., 1994).
[19] G.F. Bertsch and K. Yabana, *Phys. Rev. A* **49** (1994) 1930.
[20] K. Yabana and G.F. Bertsch, *J. Chem. Phys.* **100** (1994) 5580.
[21] G. Bertsch, N. Onishi and K. Yabana, *Z. Phys. D* **34** (1995) 213.
[22] G.F. Bertsch, A. Smith and K. Yabana, *Phys. Rev. B* **52** (1995) 7876.
[23] K. Yabana and G.F. Bertsch, *Z. Phys. D* **32** (1995) 329.
[24] K. Yabana and G.F. Bertsch, *Phys. Rev. B* **54** (1996) 4484.
[25] K. Yabana and G.F. Bertsch, *Zeit. Phys. D* **42** (1997) 219.
[26] K. Yabana and G.F. Bertsch, *Phys. Rev. A* **58** (1998) 2604.
[27] K. Yabana and G.F. Bertsch, *Phys. Rev. A* **60** (1999) 1271.
[28] K. Yabana and G.F. Bertsch, *Phys. Rev. A* **60** (1999) 3809.
[29] K. Yabana and G.F. Bertsch, *Int. J. Quant. Chem.* **75** (1999) 55.
[30] K. Yabana, G.F. Bertsch and A. Rubio, preprint arXiv: phys/0003090.
[31] G.F. Bertsch, J.-I. Iwata, A. Rubio and K. Yabana, preprint arXiv: cond-mat/0005512.
[32] V. Weisskopf, *Phys. Rev.* **52** (1937) 295.
[33] L.S. Kassel, *J. Chem. Phys.* **32** (1928) 225; **32** (1928) 1065.
[34] P.C. Engelking, *J. Chem. Phys.* **87** (1987) 3784.
[35] J.M. Weber, K. Hansen, M. Ruf and H. Hotop, *Chem. Phys.* **239** (1998) 271.
[36] C. Walther *et al.*, *Phys. Rev. Lett.* **83** (1999) 3816.
[37] J.U. Anderson *et al.*, *Phys. Rev. Lett.* **77** (1996) 3991.
[38] B. Weber and R. Scholl, *A. Appl. Phys.* **74** (1993) 607.
[39] K. Hansen and E. Campbell, *Phys. Rev. E* **58** (1998) 5477.
[40] H. Flocard, S. Koonin and M. Weiss, *Phys. Rev. C* **17** (1978) 1682.
[41] J.P. Perdew, K. Burke and M. Ernzerhof, *Phys. Rev. Lett.* **77** (1996) 3865.
[42] J.P. Perdew, S. Kurth, A. Zupan and P. Blaha, *Phys. Rev. Lett.* **82** (1999) 2544.
[43] L. Hedin, *J. Phys. Cond. Matt.* **11** (1999) R489.
[44] A. Fetter and J.D. Walecka, *Quantum Theory of Many-Particle Systems* (McGraw-Hill, N.Y., 1971).
[45] A.D. Becke, *Phys. Rev. A* **38** (1988) 3098.
[46] J. Kohanoff *et al.*, *Phys. Rev. B* **46** (1992) 4371.
[47] A. Zangwill and P. Soven, *Phys. Rev. A* **21** (1980) 1561.
[48] M. Madjet, C. Guet and W.R. Johnson, *Phys. Rev. A* **51** (1995) 1327.
[49] S.G. Louie, S. Froyen and M.L. Cohen, *Phys. Rev. B* **26** (1982) 1738.
[50] S.A. Blunden and C. Guet, *Z. Phys. D* **33** (1995) 153.
[51] C. Brechignac *et al.*, *Phys. Rev. Lett.* **70** (1993) 2036.

[52] A. Liebsch, *Phys. Rev. Lett.* **71** (1993) 145.
[53] J. Tiggesbäumker *et al.*, *Chem. Phys. Lett.* **190** (1992) 42.
[54] D. Forney *et al.*, *J. Chem. Phys.* **104** (1996) 4954.
[55] K. Chang and W. Graham, *J. Chem. Phys.* **77** (1982) 4300.
[56] B. Champagne *et al.*, *J. Phys. Chem.* **104** (2000) 4755.
[57] M. Rohlfing and S.G. Louie, *Phys. Rev. Lett.* **82** (1999) 1959.
[58] H. Perkampus, *UV Atlas of organic compounds*, Vol. 1 (Butterworth Verlag Chemie, 1968).
[59] J.W. Mintmire and C.T. White, *Phys. Rev. Lett.* **81** (1998) 2506.
[60] P. Kim, T. Odom, J.L. Huang and C.M. Lieber, *Phys. Rev. Lett.* **82** (1999) 1225.
[61] S. Frank *et al.*, *Science* **280** (1998) 1745.